A novel Netrin-1–sensitive mechanism promotes local SNARE-mediated exocytosis during axon branching

Cortney C. Winkle,[1] Leslie M. McClain,[4] Juli G. Valtschanoff,[1,2] Charles S. Park,[2] Christopher Maglione,[2] and Stephanie L. Gupton[1,2,3]

[1]Neuroscience Center and Curriculum in Neurobiology, [2]Department of Cell Biology and Physiology, and [3]Lineberger Comprehensive Cancer Center, University of North Carolina at Chapel Hill, Chapel Hill, NC 27599
[4]The David H. Koch Institute for Integrative Cancer Research, Massachusetts Institute of Technology, Cambridge, MA 02139

Developmental axon branching dramatically increases synaptic capacity and neuronal surface area. Netrin-1 promotes branching and synaptogenesis, but the mechanism by which Netrin-1 stimulates plasma membrane expansion is unknown. We demonstrate that SNARE-mediated exocytosis is a prerequisite for axon branching and identify the E3 ubiquitin ligase TRIM9 as a critical catalytic link between Netrin-1 and exocytic SNARE machinery in murine cortical neurons. TRIM9 ligase activity promotes SNARE-mediated vesicle fusion and axon branching in a Netrin-dependent manner. We identified a direct interaction between TRIM9 and the Netrin-1 receptor DCC as well as a Netrin-1–sensitive interaction between TRIM9 and the SNARE component SNAP25. The interaction with SNAP25 negatively regulates SNARE-mediated exocytosis and axon branching in the absence of Netrin-1. Deletion of *TRIM9* elevated exocytosis in vitro and increased axon branching in vitro and in vivo. Our data provide a novel model for the spatial regulation of axon branching by Netrin-1, in which localized plasma membrane expansion occurs via TRIM9-dependent regulation of SNARE-mediated vesicle fusion.

Introduction

In the developing nervous system, axons branch to innervate multiple targets. The human brain contains an estimated 10^{14} synaptic connections compared with 10^{11} neurons (Drachman, 2005); this 1,000-fold difference highlights the critical importance of sufficient axonal arborization. In contrast, exuberant axonal arborization and inappropriate innervation is implicated in neurodevelopmental disorders including autism and epilepsy (Swann and Hablitz, 2000; Zikopoulos and Barbas, 2013), emphasizing the necessity of regulated branching. Spatiotemporal control of branching is orchestrated by extracellular guidance cues, such as Netrin-1, which promote axon branching (Kennedy and Tessier-Lavigne, 1995; Dent et al., 2004). Mutations and variation in the Netrin-1 receptor *deleted in colorectal cancer* (*DCC*) are implicated in synaptic mistargeting and neurological conditions, including mirror movement disorder and schizophrenia (Srour et al., 2010; Grant et al., 2012). Although Netrin-1–dependent axonal arborization involves substantial plasma membrane expansion, how new membrane material is inserted into the plasma membrane in response to Netrin-1 is unknown. Membrane addition likely occurs via exocytic vesicle fusion, the minimal requirement of which is the formation of a SNARE complex. The SNARE complex comprises a v-SNARE, such as VAMP2 (vesicle-associated membrane protein 2), and plasma membrane t-SNAREs, Syntaxin-1 and SNAP25 (synaptosomal-associated protein 25; Söllner et al., 1993; Hayashi et al., 1994). Although SNARE complex formation is required for vesicle fusion and neurotransmitter release at the synapse (Südhof, 2012), the role of SNARE-mediated exocytosis in axon branching has not been defined.

In *Caenorhabditis elegans* and *Drosophila melanogaster*, the *NTN1* and *DCC* orthologues *unc-6/netrin* and *unc-40/frazzled* promote axon development through *madd-2/asap*, the single

Correspondence to Stephanie L. Gupton: sgupton@email.unc.edu

Abbreviations used in this paper: ANOVA, analysis of variance; BoNTA, botulinum toxin A; CC, coiled coil; CMV, cytomegalovirus; DCC, deleted in colorectal cancer; DIC, differential interference contrast; LD, ligase dead; ROI, region of interest; TeNT, tetanus toxin; TIRF, total internal reflection fluorescence; TRIM, tripartite motif.

The Rockefeller University Press $30.00
J. Cell Biol. Vol. 205 No. 2 217–232
www.jcb.org/cgi/doi/10.1083/jcb.201311003

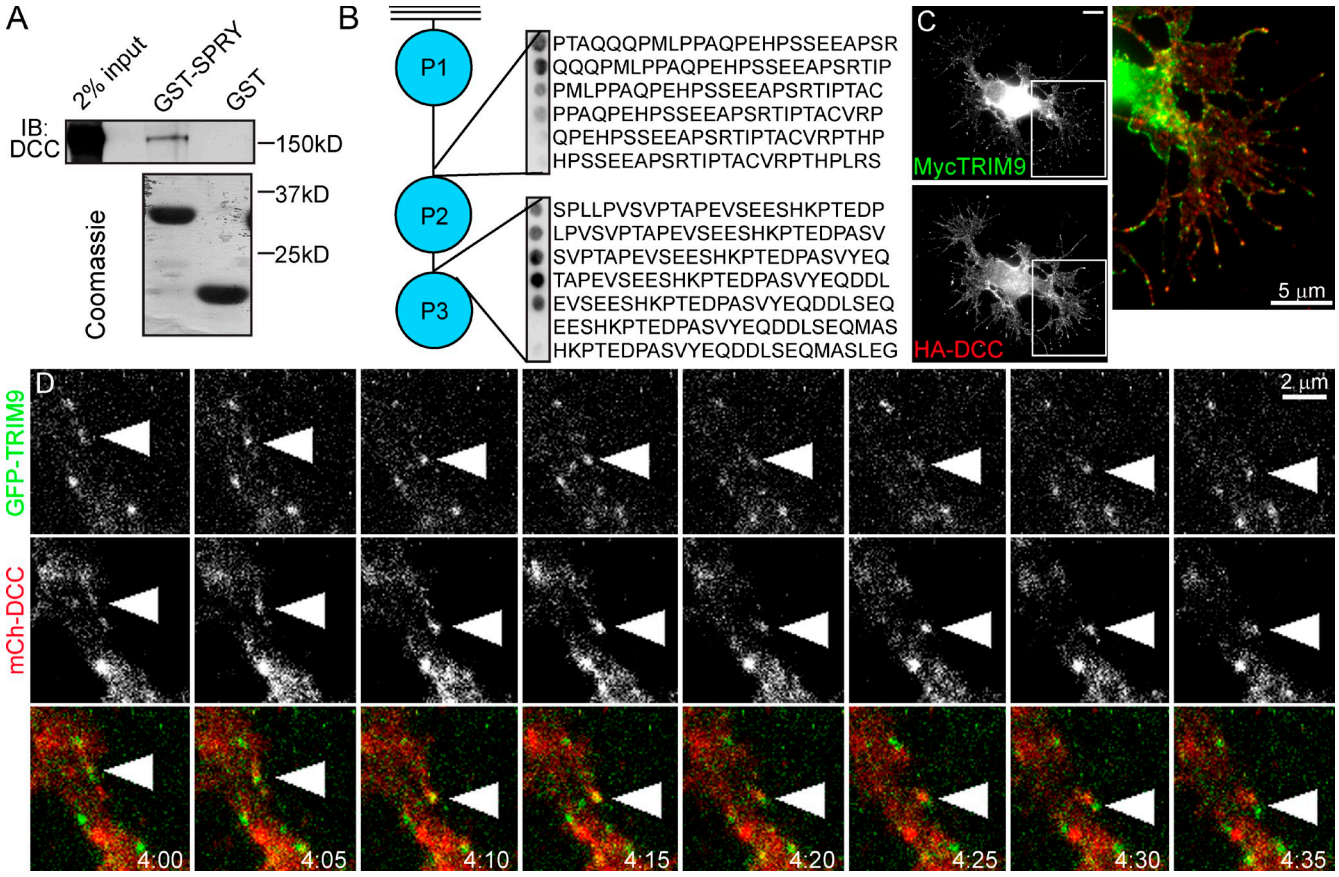

Figure 1. **TRIM9 directly binds the Netrin-1 receptor DCC and colocalizes with DCC in cortical neurons.** (A) Bacterially expressed GST-SPRY domain interacts with DCC in embryonic mouse cortical lysate. Protein purity is shown by Coomassie. IB, immunoblot. (B) Sequential overlapping peptides within the cytoplasmic tail of DCC were arrayed on nitrocellulose and probed with GST-SPRY, GST antibodies, and HRP secondary antibodies. The SPRY domain binds two sequences within the cytoplasmic tail of DCC. (C) E15.5 cortical neuron transfected with MycTRIM9 and HA-DCC and cultured for 48 h. Boxes denotes the ROIs shown in the enlarged color-combined image. (D) Neuron transfected with GFP-TRIM9 and mCherry (mCh)-DCC imaged by TIRF. Arrowheads denote colocalization, and time is given in seconds (Video 1).

invertebrate orthologue of class I tripartite motif (TRIM) E3 ubiquitin ligases (Hao et al., 2010; Morikawa et al., 2011). Evolutionary conservation of netrin pathway components suggests that the closest vertebrate orthologue TRIM9 (Hao et al., 2010; Morikawa et al., 2011) might regulate axon development downstream of Netrin-1. Intriguingly, vertebrate TRIM9 was identified as a binding partner of the t-SNARE SNAP25 (Li et al., 2001), but whether this interaction is relevant in developing neurons is unknown.

TRIM E3 ubiquitin ligases share a conserved N-terminal TRIM motif, comprising a ubiquitin ligase RING (really interesting gene) finger, one to two BBox domains, and a coiled-coil (CC) motif followed by diverse C termini that distinguish TRIM classes (Meroni and Diez-Roux, 2005). Mutation of single vertebrate TRIM genes results in unique phenotypes and human diseases (Gaudenz et al., 1998; Hämäläinen et al., 2004; Saccone et al., 2008; Hatakeyama, 2011). This is likely caused by the expression and substrate specificity of individual TRIMs. TRIM9 is expressed in the adult and developing nervous system and exhibits ligase activity in vitro, although its substrates in vivo have not been identified (Berti et al., 2002; Tanji et al., 2010). Despite the aforementioned phylogenetic clues, the role of vertebrate TRIM9 in Netrin-1–dependent axon branching and SNARE-mediated exocytosis remains to be examined.

Here, we identify a novel mechanism by which TRIM9 spatially controls SNARE-mediated exocytosis to promote Netrin-1–dependent axon branching in murine cortical neurons. We show that TRIM9 directly binds to the cytoplasmic tail of DCC and that TRIM9 ligase activity is required to impart sensitivity to Netrin-1 in cortical neurons. We demonstrate that the TRIM9 interaction with SNAP25 inhibits SNARE complex formation, vesicle fusion, and axon branching in the absence of Netrin-1. We find that TRIM9 releases SNAP25 after Netrin-1 stimulation and that this release promotes Netrin-1–dependent SNARE-mediated vesicle fusion and axon branching. After deletion of *TRIM9*, cortical neurons exhibit exaggerated exocytosis and branching along with a loss of Netrin-1 responsiveness. The exuberant branching that occurs in the absence of *TRIM9* in vitro is also observed in axons crossing the corpus callosum, highlighting in vivo the relevance of the mechanism identified here. Interactions with DCC and SNAP25 uniquely position TRIM9 at the interface of Netrin-1 signaling and exocytosis, allowing TRIM9 to spatially coordinate vesicle trafficking, membrane expansion, and axon branching in a Netrin-1–dependent manner.

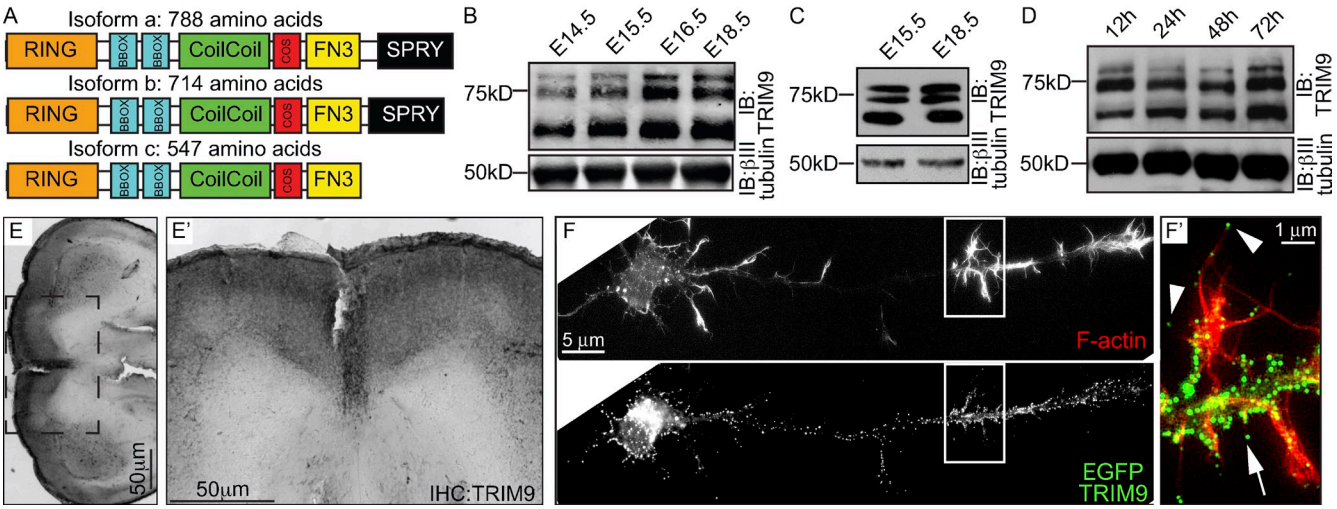

Figure 2. **TRIM9 is expressed in the developing murine cortex.** (A) Murine TRIM9 isoforms. COS, C-terminal subgroup one signature. (B–D) Immunoblots (IB) using a TRIM9 polyclonal antibody demonstrate TRIM9 expression in embryonic whole brain lysate (B), in embryonic cortex (C), and in cortical neurons (D) cultured for the indicated times. βIII-Tubulin is a loading control. The data shown in C are shown again in Fig. S2 E alongside *TRIM9*$^{-/-}$ samples. (E and E′) Immunohistochemistry (IHC) of E15.5 brain using TRIM9 monoclonal antibody (black) reveals TRIM9 expression in the developing cortex. The dotted square is the ROI shown in E′. (F and F′) EGFP-TRIM9 localizes to punctae at the periphery of the cell body, along the axon shaft (arrow) and at the tips of F-actin–positive filopodia (arrowheads; F′); phalloidin is shown in red. Boxes show the ROI represented in the enlarged color-combined image in F′.

Results

Vertebrate TRIM9 binds to and colocalizes with the Netrin-1 receptor DCC

Netrin-1 and DCC direct axon guidance in the invertebrate and vertebrate nervous systems (Kennedy and Tessier-Lavigne, 1995). DCC, which lacks catalytic function, initiates Netrin-1–dependent signaling pathways via cytoplasmic interaction partners (Round and Stein, 2007). Based on phylogenetic conservation with invertebrate regulators of netrin-dependent axon guidance (Alexander et al., 2010; Hao et al., 2010; Morikawa et al., 2011), we hypothesized that vertebrate TRIM9 may regulate Netrin-1 responses in the developing nervous system. To determine whether TRIM9 interacted with DCC, we incubated bacterially expressed and purified GST-SPRY (SplA/ryanodine) domain of human TRIM9 in lysates prepared from embryonic day 15.5 (E15.5) mouse cortex and analyzed bound proteins by SDS-PAGE and immunoblotting (Fig. 1 A). GST-SPRY, but not GST alone, bound endogenous DCC, indicating that the SPRY domain of vertebrate TRIM9 was able to interact with DCC in neurons.

To determine whether this interaction was direct and to elucidate the binding site within DCC, we probed an overlapping sequential peptide array of the cytoplasmic tail of DCC with GST-SPRY (Fig. 1 B). GST-SPRY bound two sequences within the cytoplasmic tail of DCC, demonstrating that TRIM9 directly binds DCC. This was confirmed by directed yeast two-hybrid techniques (unpublished data). To characterize TRIM9 and DCC localization, we introduced epitope-tagged expression constructs into cortical neurons. TRIM9 and DCC exhibited significant colocalization at tips of neurites and growth cone extensions (Pearson's correlation coefficient of 0.55 ± 0.03 vs. 0.02 of rotated images, $P < 0.01$; Fig. 1 C). Furthermore, GFP-TRIM9 and mCherry-DCC dynamically colocalized within the axonal shaft of cortical neurons (Fig. 1 D and Video 1). Thus, mammalian TRIM9 is a bona fide DCC binding partner that colocalizes with DCC in developing cortical neurons.

TRIM9 is expressed in the developing cortex

To determine whether TRIM9 is expressed in the embryonic cortex where Netrin-1/DCC functions are established, we raised an antibody against the highly conserved BBox domains of TRIM9. Three predicted isoforms of murine TRIM9 (Fig. 2 A) were recognized in lysates prepared from embryonic whole brain, embryonic cortex, and cultured embryonic cortical neurons (Fig. 2, B–D). Immunohistochemistry of the E15.5 brain further demonstrated TRIM9 expression specifically in the developing cortex (Fig. 2 E). To determine whether TRIM9 localized to F-actin–rich structures in cortical neurons, we expressed GFP-TRIM9 and costained F-actin with fluorescent phalloidin. GFP-TRIM9 localized to puncta at the cell body periphery, along the axon, and to filopodial tips (Fig. 2 F). Using two different polyclonal antibodies, we found endogenous TRIM9 similarly localized to phalloidin-stained filopodia tips (Fig. S1, A and B).

TRIM9 function is required for Netrin-1–dependent axon branching

Netrin-1 stimulation robustly increases axon branching in cortical neurons (Dent et al., 2004), which we hypothesized involved TRIM9. To examine this, we adopted a dominant-negative approach (Fig. 3). RING deletion mutants (ΔRING) of ubiquitin ligases will dimerize with the endogenous ligase and block substrate ubiquitination (Kubbutat and Vousden, 1997; Yang et al., 2000; Tursun et al., 2005). Consistent with this, MycTRIM9ΔRING coimmunoprecipitated GFP-TRIM9 (Fig. S1 C), and expression of madd-2ΔRING phenocopied defects observed in *madd-2* mutant worms (Hao et al., 2010). Neurons were transfected with Myc

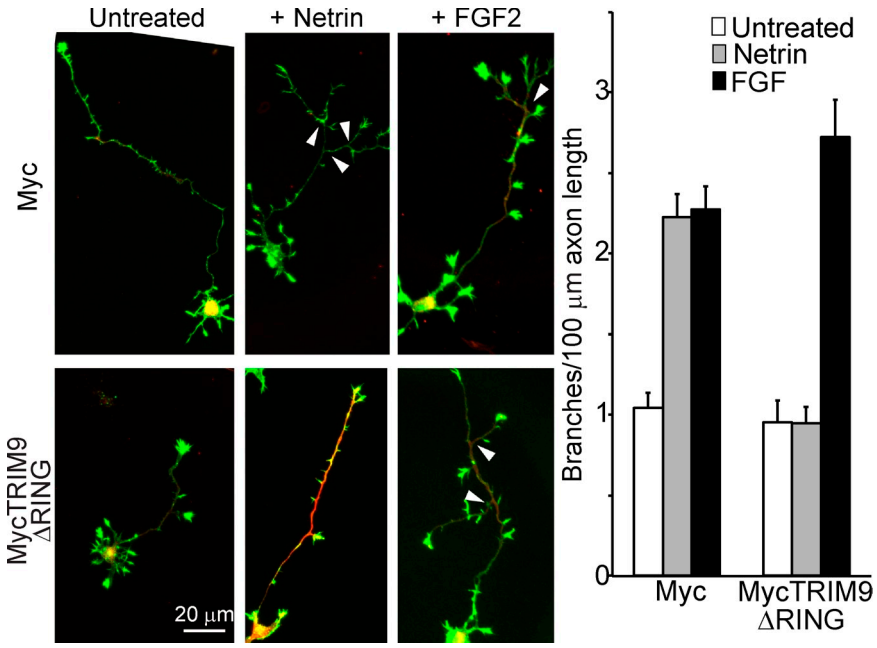

Figure 3. **TRIM9 ubiquitin ligase function is required for Netrin-1–dependent axon branching.** E15.5 cortical neurons transfected with Myc or MycTRIM9ΔRING (red) stained with phalloidin to mark F-actin (green) in Netrin-1 and FGF2 branching assays. Arrowheads denote axon branching points. Mean axon branch density ± SEM; *n* = 593 neurons. P-values were obtained from ANOVA with Tukey's post-hoc analysis.

or MycTRIM9ΔRING expression plasmids, cultured 48 h, and stimulated with Netrin-1 (Fig. 3). Myc-expressing neurons exhibited a significant increase in axon branching compared with unstimulated neurons, whereas MycTRIM9ΔRING-expressing neurons failed to increase axon branch density in response to Netrin-1. This suggests that TRIM9 ligase activity is required for Netrin-1–dependent axon branching. To determine whether TRIM9 regulation of branching was Netrin-1 specific, we stimulated neurons with FGF2 (fibroblast growth factor 2; Fig. 3). Unlike Netrin-1, FGF2 promotes axon branching in a FGF2 receptor–dependent manner (Reuss and von Bohlen und Halbach, 2003; Zechel et al., 2010). Both Myc- and MycTRIM9ΔRING-expressing neurons increased axon branch density in response to FGF2; thus, TRIM9 ligase function is specifically required for axon branching downstream of Netrin-1.

Genetic loss of *TRIM9* leads to exaggerated axon branching

To further elucidate the function of TRIM9, we generated a conditional *TRIM9* allele (Fig. S2 A). Mice carrying this allele were crossed with cytomegalovirus (CMV)-Cre mice to generate *TRIM9*$^{-/-}$ mice, which were born at Mendelian ratios (Fig. S2, B and C). Analysis of whole brain, cortex, and cultured cortical neurons isolated from *TRIM9*$^{-/-}$ embryos and cortical tissue from *TRIM9*$^{-/-}$ adults confirmed the loss of TRIM9 immunoreactivity (Fig. S2, D–G). Reduced immunoreactivity was observed by immunocytochemistry and was absent from filopodia tips (Fig. S1, A and B). We next tested *TRIM9*$^{-/-}$ cortical neurons in axon branching assays (Fig. 4 A). Although *TRIM9*$^{+/+}$ neurons significantly increased axon branching after Netrin-1 stimulation, *TRIM9*$^{-/-}$ neurons exhibited significantly higher constitutive axon branching, and Netrin-1 stimulation did not elevate axon branching further (Fig. 4 B). These defects were corroborated in an independent line of *TRIM9*$^{-/-}$ mice (Fig. S2 H). These results indicate that TRIM9 minimizes constitutive axon branching and imparts Netrin-1 sensitivity.

To confirm that aberrant axon branching was caused by loss of *TRIM9*, we introduced MycTRIM9 expression plasmids into *TRIM9*$^{-/-}$ neurons (Fig. 4 B and Fig. S3). MycTRIM9 expression decreased constitutive branching to wild-type levels and restored Netrin-1 sensitivity, rescuing the aberrant branching of *TRIM9*$^{-/-}$ neurons. To define the role of TRIM9 ligase activity, we introduced MycTRIM9ΔRING or a ligase-dead (LD) mutant (TRIM9LD; Fig. 4 B and Fig. S3). Mutation of the first two conserved cysteines renders TRIM proteins catalytically inactive (Joazeiro and Weissman, 2000; Balastik et al., 2008; Hung et al., 2010). Expression of either MycTRIM9ΔRING or MycTRIM9LD reduced the exaggerated constitutive axon branching exhibited by *TRIM9*$^{-/-}$ neurons, indicating that ligase activity is not essential to restrict constitutive axon branching. However, these mutants failed to restore Netrin-1–dependent axon branching, suggesting that ligase activity is necessary for Netrin-1 sensitivity. In contrast to invertebrates, these data indicate that expression of TRIM9ΔRING does not fully phenocopy *TRIM9* deletion and is suggestive of divergence of TRIM9 orthologues.

To determine whether TRIM9 function was required specifically for response to Netrin-1, we stimulated *TRIM9*$^{-/-}$ neurons with 10 ng/ml FGF2 (Fig. 4 C), which failed to promote axon branching (Fig. 4 D). We hypothesized that this failure to respond to FGF2 may occur if axon branching were at a maximum. Consistent with this, expression of TRIM9ΔRING in *TRIM9*$^{-/-}$ neurons reduced constitutive axon branching levels and rescued the branching response to FGF2 (Fig. 4 D). Thus, in contrast to Netrin-1, TRIM9 ligase activity is dispensable for axon branching in response to FGF2. Unlike axon branching, Netrin-1 stimulation or loss of *TRIM9* did not alter axon length (Fig. 4 E).

TRIM9 regulates Netrin-1–induced SNARE-mediated exocytosis

Axon branching increases plasma membrane surface area, necessitating the addition of new membrane material (Pfenninger, 2009), likely via SNARE-mediated exocytosis. To determine

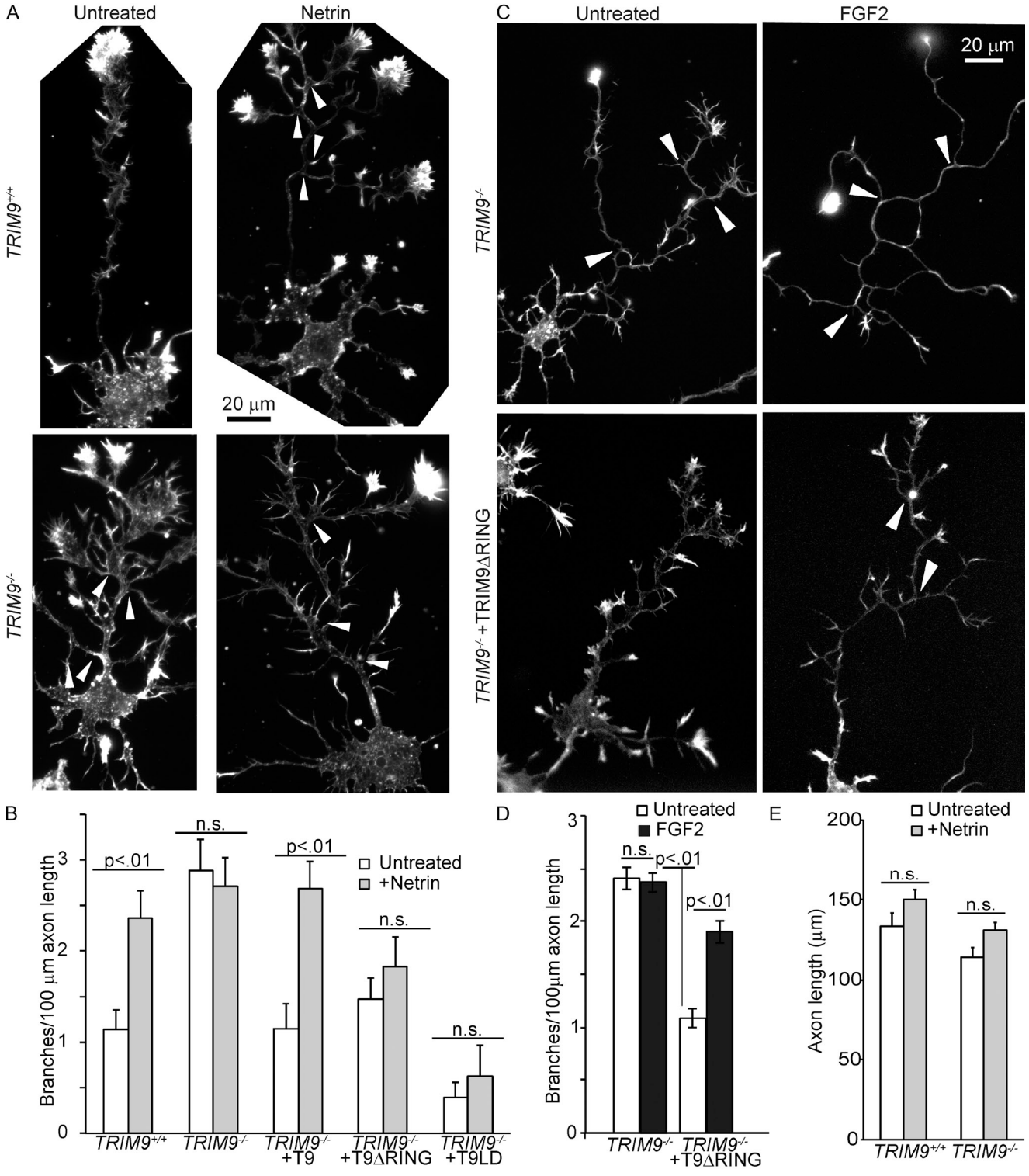

Figure 4. **TRIM9 is required for Netrin-1–dependent branching.** (A) E15.5 *TRIM9*$^{+/+}$ and *TRIM9*$^{-/-}$ cortical neurons were untreated or Netrin-1 stimulated and stained with fluorescent phalloidin. Arrowheads denote branch points. (B) Mean axon branch density ± SEM. $n > 80$ neurons/condition. Expression of Myc-TRIM9 (T9) in *TRIM9*$^{-/-}$ neurons reduced constitutive branching and rescued Netrin-1 sensitivity. MycTRIM9ΔRING (T9ΔRING) or MycTRIM9LD (T9LD) introduction failed to rescue Netrin-1–dependent branching. (C) E15.5 *TRIM9*$^{-/-}$ cortical neurons expressing either Myc or MycTRIM9ΔRING were untreated or FGF2 stimulated and stained with fluorescent phalloidin and antibodies to Myc and βIII-tubulin (not depicted). Arrowheads denote branch points. (D) Mean axon branch density ± SEM. Stimulation of *TRIM9*$^{-/-}$ neurons with FGF2 fails to increase already exaggerated axon branching except in cells expressing MycTRIM9ΔRING. (E) Axon length is not affected by Netrin-1 or genetic loss of *TRIM9*. Means ± SEM. All graphs are $n > 80$ neurons/condition from more than three independent experiments. P-values were obtained from ANOVA with Tukey's post-hoc analysis.

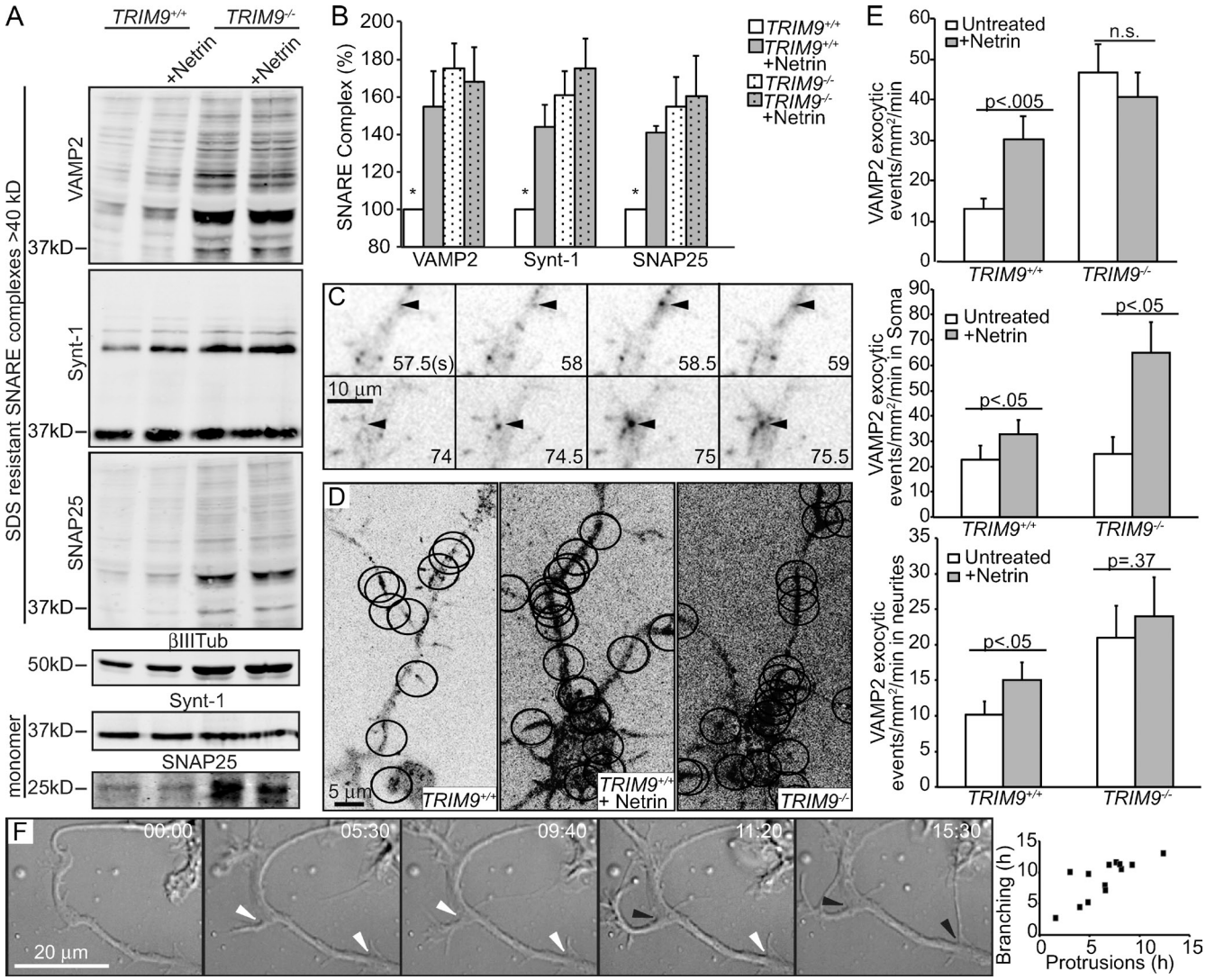

Figure 5. **TRIM9 regulates SNARE complex formation and exocytosis.** (A) Immunoblot showing SDS-resistant SNARE complexes in *TRIM9*$^{+/+}$ and *TRIM9*$^{-/-}$ cortical neurons probed for VAMP2, Syntaxin-1a (Synt-1), and SNAP25. βIII-Tubulin (Tub) is a loading control. Syntaxin-1 and SNAP25 monomer are shown in boiled samples; $n = 3$ independent experiments. These samples are shown again in Fig. S4 A alongside boiled samples. (B) Quantitation of SNARE complexes (>40 kD) was normalized to βIII-tubulin. Significance is from ANOVA with Tukey's post-hoc analysis; *, $P < 0.5$. (C) Inverted image montage of VAMP2-pHluorin exocytosis events in TIRF images. Arrowheads denote exocytic events, and time is noted in seconds. (D) Maximal projections of VAMP2-phluorin time lapse. Ovals denote location of exocytic events within 90 s (Videos 2 and 3). (E) Mean frequency of VAMP2-pHluorin exocytosis events ± SEM; $n \geq 10$ cells/condition. P-value was obtained from Kruskal–Wallis nonparametric ANOVA within the entire image (top), soma (middle), or neurites (bottom). (F) DIC image montage showing the initial plasma membrane protrusion and subsequent axon branch formation of a *TRIM9*$^{+/+}$ cortical neuron after Netrin-1 stimulation (time is in hours and minutes). White arrowheads denote active plasma membrane protrusions; black arrowheads denote axon branches ≥20 µm long (Video 4). Scatter plot shows the time of initial axon protrusions at future branch sites in hours after Netrin-1 stimulation plotted against the time a stable 20-µm-long branch appears after Netrin-1 stimulation; $n = 13$ cells. Error bars show SEMs.

whether Netrin-1 stimulation elevated the formation of SNARE complexes associated with exocytosis, we exploited the SDS resistance of SNARE complexes (Fig. 5 A and Fig. S4 A). In *TRIM9*$^{+/+}$ neurons, the quantity of SNARE complexes (>40 kD) was significantly increased after 1 h of Netrin-1 stimulation (Fig. 5, A and B). Like axon branching, basal SNARE complex levels were higher in *TRIM9*$^{-/-}$ neurons (Fig. 5, A and B), consistent with the finding that TRIM9 binds SNAP25 (Li et al., 2001) and blocks the interaction between SNAP25 and VAMP2. Notably, no further increase in SNARE complex formation occurred after Netrin-1 stimulation, suggesting that TRIM9 is required for Netrin-1–sensitive SNARE complex formation.

Elevated SNARE complex formation does not necessarily signify increased rates of exocytosis. To define effects on SNARE-mediated vesicle fusion, we expressed VAMP2 tagged with the pH-sensitive GFP variant pHluorin (Miesenböck et al., 1998) and performed total internal reflection fluorescence (TIRF) time-lapse microscopy to track the frequency of exocytic events (Fig. 5, C–E; and Videos 2 and 3). The basal frequency of VAMP2-mediated exocytosis in *TRIM9*$^{+/+}$ neurons increased after Netrin-1 stimulation, as demonstrated by time-lapse imaging and maximal projections (Fig. 5, D and E; and Video 2). In line with elevated SNARE complex formation, *TRIM9*$^{-/-}$ cortical neurons exhibited a threefold increase in the frequency of exocytic events compared

with *TRIM9*$^{+/+}$ neurons (Fig. 5, D and E; and Video 3). Exocytic frequency was not increased further by Netrin-1 and corroborated a role for TRIM9 in constraining SNARE-mediated exocytosis and providing Netrin-1 sensitivity.

To determine whether TRIM9 regulated exocytosis spatially, we compared the frequency of exocytic events in the soma and neurites (Fig. 5 E). The frequency of exocytic events in the soma was unchanged in *TRIM9*$^{-/-}$ compared with *TRIM9*$^{+/+}$ neurons, and both increased significantly in response to Netrin-1, indicating that TRIM9 does not constrain exocytosis in the soma. However, exocytic frequency was significantly elevated in the neurites of *TRIM9*$^{-/-}$ neurons and did not further increase in response to Netrin-1, unlike *TRIM9*$^{+/+}$ neurons. Thus, TRIM9 spatially restricts exocytosis in neurites, but not the soma, of cortical neurons in the absence of Netrin-1.

These data suggested that Netrin-1–dependent axon branching was preceded by elevated exocytosis. To determine the time course of Netrin-1–dependent branching, *TRIM9*$^{+/+}$ neurons were imaged by differential interference contrast (DIC) time-lapse microscopy (Fig. 5 F and Video 4). Increased growth cone protrusions and altered filopodial dynamics were apparent within 1 h of Netrin-1 stimulation. In contrast, membrane protrusion at future axon branch sites began 6.5 ± 0.8 h after Netrin-1 stimulation (Fig. 5 F). Stable branches appeared at these sites 2.5 ± 0.6 h after initial protrusion activity. Thus, increased SNARE-mediated exocytosis, which occurs within 1 h of Netrin-1 stimulation, precedes axonal membrane protrusion and subsequent axon branching.

SNARE-mediated exocytosis is required for axon branching

The increase in exocytosis after Netrin-1 stimulation or genetic loss of *TRIM9* suggested that SNARE-mediated exocytosis is required for axon branching. Because TRIM9 binds SNAP25, we anticipated that SNAP25-mediated exocytosis was critical. To demonstrate a requirement for SNAP25 during axon branching, we treated *TRIM9*$^{+/+}$ neurons with 10 nM botulinum toxin A (BoNTA; Fig. 6 A), which cleaves SNAP25 (Schiavo et al., 1993). BoNTA treatment blocked Netrin-1–dependent branching (Fig. 6 B). We similarly treated *TRIM9*$^{+/+}$ neurons with tetanus toxin (TeNT), which cleaves VAMP2 and blocks VAMP2-mediated exocytosis (Schiavo et al., 1992). Surprisingly, TeNT treatment did not inhibit Netrin-1–dependent axon branching. VAMP7 is a neuronal v-SNARE that also forms a SNARE complex with SNAP25 (Martinez-Arca et al., 2000). To determine whether VAMP7 was required for branching, we expressed the longin domain of VAMP7, which inhibits VAMP7-mediated exocytosis (Martinez-Arca et al., 2000; Gupton and Gertler, 2010). This also failed to block Netrin-1–dependent axon branching in *TRIM9*$^{+/+}$ neurons (Fig. 6, A and B), indicating that neither VAMP2 nor VAMP7 independently are required for axon branching. In contrast, simultaneous inhibition of VAMP2- and VAMP7-mediated exocytosis, by treating longin-expressing neurons with TeNT, blocked Netrin-1–dependent axon branching, indicating a requirement for VAMP2- or VAMP7-mediated exocytosis. To determine whether aberrant exocytosis induced the exuberant axon branching of *TRIM9*$^{-/-}$ neurons, we similarly treated *TRIM9*$^{-/-}$ neurons with BoNTA (Fig. 6 C). BoNTA treatment reduced elevated axon branching of *TRIM9*$^{-/-}$ neurons to wild-type levels (Fig. 6 D), indicating SNARE-mediated exocytosis is required for the exuberant branching phenotype of *TRIM9*$^{-/-}$ neurons.

The TRIM9–SNAP25 interaction is Netrin-1 sensitive

If TRIM9 constrained exocytosis by interacting with SNAP25, we hypothesized that Netrin-1 stimulation would induce the release of SNAP25 to promote exocytosis. To examine TRIM9–SNAP25 binding, we used coimmunoprecipitation assays in HEK293 cells expressing MycTRIM9, GFP-SNAP25B, and HA-DCC to impart Netrin-1 sensitivity (Fig. 7 B). MycTRIM9 coimmunoprecipitated GFP-SNAP25 in the absence of Netrin-1, and the levels of GFP-SNAP25 coimmunoprecipitated with MycTRIM9 were significantly reduced by Netrin-1 stimulation (Fig. 7 B). To determine whether residual SNAP25 bound to MycTRIM9 in the presence of Netrin-1 reflected nonspecific binding, we performed several controls. Myc alone coimmunoprecipitated levels of GFP-SNAP25 indistinguishable from that bound to MycTRIM9 in the presence of Netrin-1. Similarly, low binding was observed with a TRIM9 mutant lacking the CC domain (TRIM9ΔCC; Fig. 7, A and B; and Fig. S4 B), which is the minimal domain of TRIM9 sufficient for SNAP25 binding (Li et al., 2001). These controls indicate that the residual binding of SNAP25 to MycTRIM9 that occurred in the presence of Netrin-1 was nonspecific. These experiments show that the TRIM9–SNAP25 interaction is negatively regulated by Netrin-1.

TRIM9 ligase activity promotes exocytosis in a Netrin-1–dependent manner

Loss of TRIM9 ligase activity disrupted Netrin-1–dependent axon branching (Fig. 3 and Fig. 4 B). Because our data suggested that increased exocytosis was a prerequisite for axon branching (Fig. 5 and Fig. 6), we asked whether TRIM9ΔRING expression inhibited Netrin-1–dependent exocytosis. mCherryTRIM9ΔRING-expressing neurons lacked Netrin-1–dependent increases in VAMP2-mediated exocytosis (Fig. S4 C). This same inhibition was observed with VAMP7-mediated exocytosis (Fig. S4 D), delineating a role for VAMP7 in Netrin-1 response and supporting the hypothesis that TRIM9 regulates SNARE complex formation through an inhibitory interaction with SNAP25. Failure to increase SNARE-mediated exocytosis in response to Netrin-1 was correlated with increased binding between TRIM9ΔRING and SNAP25 and a failure to release SNAP25 in response to Netrin-1 (Fig. S4, B and E). This indicates that the ligase activity of TRIM9 is likely required for Netrin-1–dependent release of SNAP25 and the promotion of SNARE-mediated exocytosis. These data show that in cortical neurons, both VAMP2- and VAMP7-containing vesicles fuse more frequently with the plasma membrane in response to Netrin-1 stimulation and that Netrin-1–stimulated exocytosis is regulated by TRIM9 ligase activity. Because TRIM9ΔRING-expressing neurons lack Netrin-1–dependent axon branching, these data also support the conclusion that exocytosis is a prerequisite of axon branching.

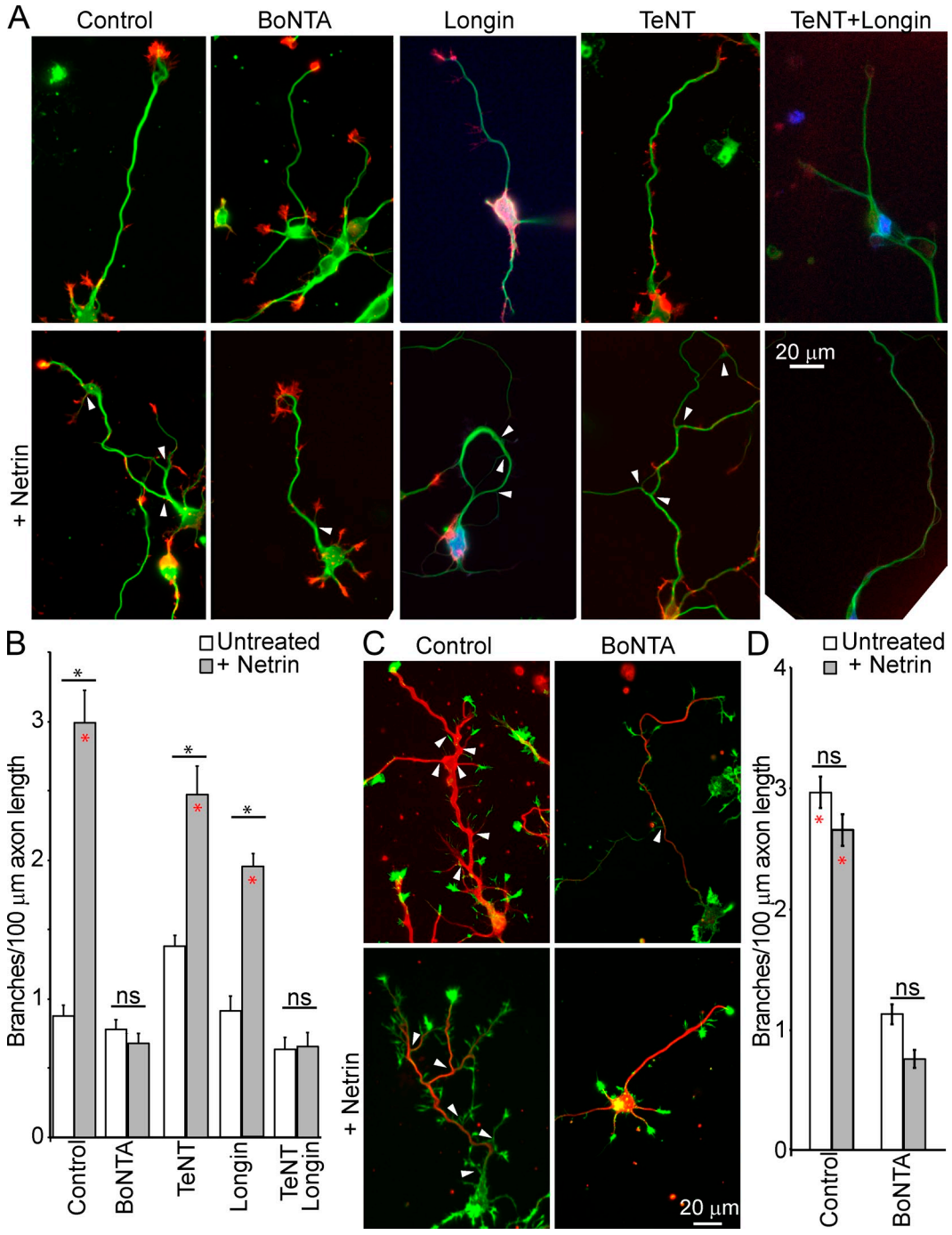

Figure 6. **SNARE proteins are required for cortical axon branching.** (A) E15.5 *TRIM9*$^{+/+}$ cortical neurons were untreated or Netrin-1 stimulated, with the addition of 10 nM BoNTA, 10 nM TeNT, and/or longin expression (blue), and stained with fluorescent phalloidin (red) and for βIII-tubulin (green). Arrowheads denote branch points. (B) Mean axon branch density ± SEM. (C) E15.5 *TRIM9*$^{-/-}$ cortical neurons were untreated or Netrin-1 stimulated, with the addition of 10 nM BoNTA, and stained with fluorescent phalloidin (red) and for βIII-tubulin (green). Arrowheads denote branch points. (D) Mean axon branch density ± SEM. Red asterisks in B and D denote statistical significance from *TRIM9*$^{+/+}$ neurons in the absence of Netrin-1 ($P < 0.5$). Black asterisks denote statistically significant differences between untreated and Netrin-1–stimulated conditions ($P < 0.5$). All graphs are at least $n > 54$ neurons/condition from more than three independent experiments (n = 1,353 neurons). P-values are from ANOVA with Tukey's post-hoc analysis.

The TRIM9 CC domain is required for constraint of exocytosis and axon branching

Our findings suggest that the SNAP25 binding capacity of TRIM9 is a key mechanism controlling SNARE complex formation, vesicle fusion, and consequent plasma membrane expansion and axonal branching. To further test this, we investigated whether expression of the TRIM9ΔCC mutant unable to bind SNAP25 (Fig. 7 A and Fig. S4 B) rescued phenotypes associated with loss of *TRIM9*. mCherryTRIM9ΔCC expression did not reduce elevated VAMP2-mediated exocytosis in *TRIM9*$^{-/-}$ cortical neurons (Fig. 7, C and D; and Video 5), nor did MycTRIM9ΔCC

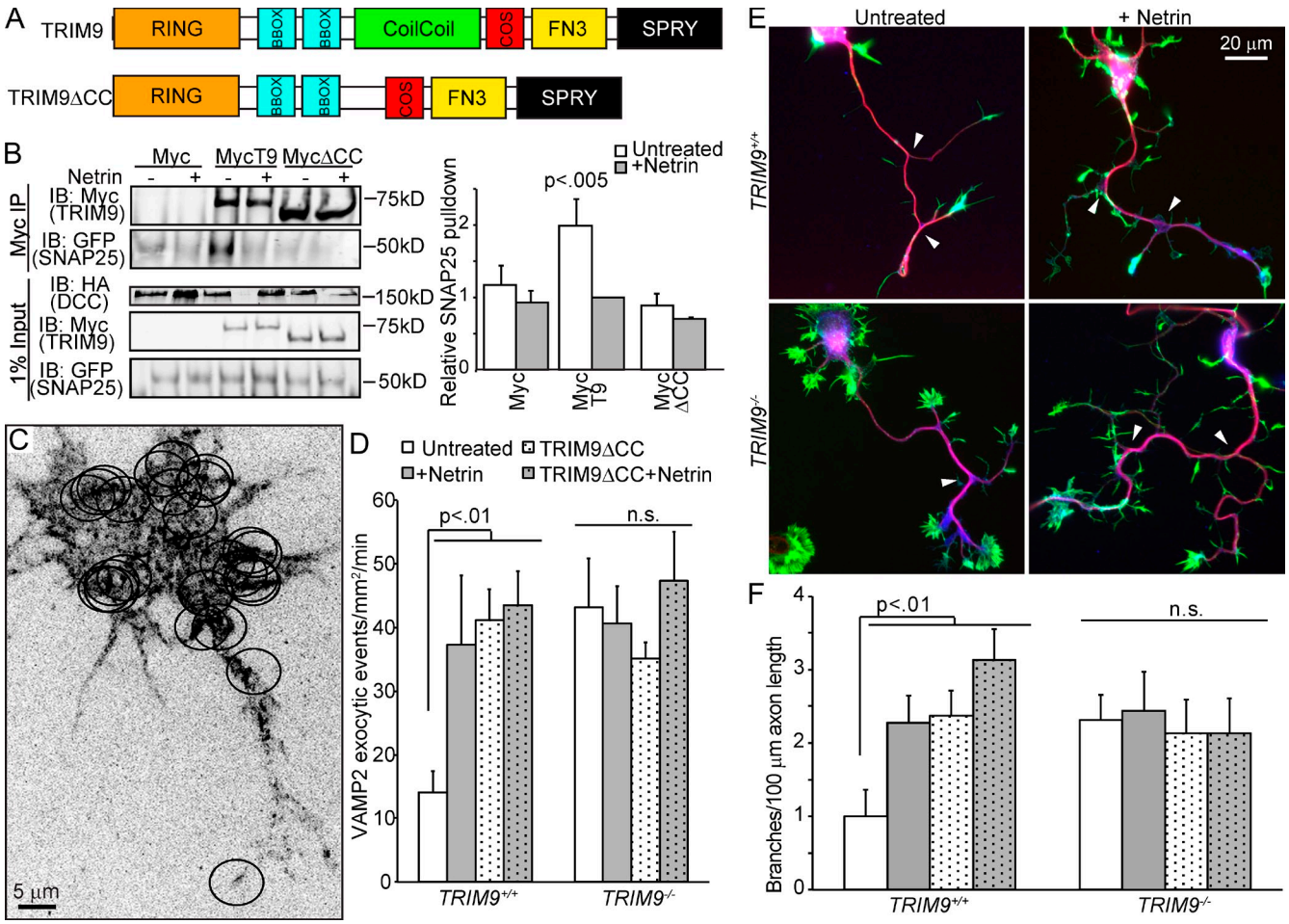

Figure 7. **The SNAP25 binding domain of TRIM9 is required to minimize exocytosis and axon branching.** (A) Domain diagram of TRIM9 and TRIM9ΔCC. COS, C-terminal subgroup one signature. (B) HEK293 cells expressing HA-DCC, GFP-SNAP25, and either Myc, MycTRIM9, or MycTRIM9ΔCC were precipitated with Myc antibody-conjugated beads ($n = 5$ independent experiments; p-values are from Kruskal–Wallis nonparametric ANOVA). The immunoblot for HA-DCC contains an empty lane between samples 3 and 4. IB, immunoblot. (C) Maximal projection of a VAMP2-pHluorin–transfected *TRIM9*$^{-/-}$ neuron expressing mCherryTRIM9ΔCC (not depicted; Video 5). Ovals denote exocytic events. (D) mCherryTRIM9ΔCC expression significantly increased VAMP2-mediated exocytic events as measured by VAMP2-pHluorin experiments in *TRIM9*$^{+/+}$, but not *TRIM9*$^{-/-}$, cortical neurons; $n \geq 10$ cells/condition. P-values are from Kruskal–Wallis ANOVA. (E) Neurons transfected with MycTRIM9ΔCC (blue) stained with phalloidin (green) and for βIII-tubulin (red) in a Netrin-1 branching assay. Arrowheads denote branches. (F) Mean axon branching density ± SEM; $n > 75$ neurons/condition from three independent experiments. P-values are from Kruskal–Wallis nonparametric ANOVA. Error bars show SEMs.

expression reduce exaggerated axon branching (Fig. 7, E and F). In light of these results and the phenotypes observed with TRIM9ΔRING expression (Fig. 3, Fig. 4 B, and Fig. S4, C–E), we conclude that the CC domain and likely SNAP25 binding of TRIM9 are required to constrain exocytosis and branching, whereas ligase activity is dispensable. Interestingly, expression of TRIM9ΔCC increased the basal frequency of VAMP2-mediated exocytic events and axon branching in *TRIM9*$^{+/+}$ neurons and was associated with a loss of Netrin-1 responsiveness (Fig. 7, D–F). The similarity in exocytic and branching phenotypes between *TRIM9*$^{-/-}$ neurons and *TRIM9*$^{+/+}$ neurons expressing TRIM9ΔCC suggests that TRIM9ΔCC acts as a dominant negative, through a mechanism other than dimerization with endogenous TRIM9 (Fig. S1 C).

Loss of *TRIM9* leads to aberrant axon branching and corpus callosum thickening

TRIM9 deletion disrupted exocytosis and axonal morphology in cortical neurons in vitro, suggesting that similar effects may occur after deletion of *TRIM9* in vivo. The corpus callosum is the largest cortical axon projection and is absent in *NTN1* and *DCC* knockout mice (Serafini et al., 1996; Fazeli et al., 1997). The callosum comprises axons extending from multiple cortical layers across the midline, where they subsequently branch and synapse within the contralateral cortex and striatum (Arlotta et al., 2005; Leyva-Díaz and López-Bendito, 2013). We stained nissl substance in coronal sections of adult *TRIM9*$^{+/+}$ and *TRIM9*$^{-/-}$ mice to visualize callosal boundaries (Fig. 8 A). This revealed that loss of *TRIM9* was associated with significant thickening of the corpus callosum, a result corroborated in a second line of *TRIM9*$^{-/-}$ mice (Fig. S5, A and B).

We hypothesized this callosal thickening may be caused by exaggerated branching of *TRIM9*$^{-/-}$ cortical axons. To investigate axon branching in vivo, we crossed *TRIM9*$^{-/-}$ mice to a line of Thy1-GFP mice. The cytoplasmic GFP expression pattern observed in Thy1-GFP mice derived from an individual founder is consistent across litters and generations (Feng et al., 2000),

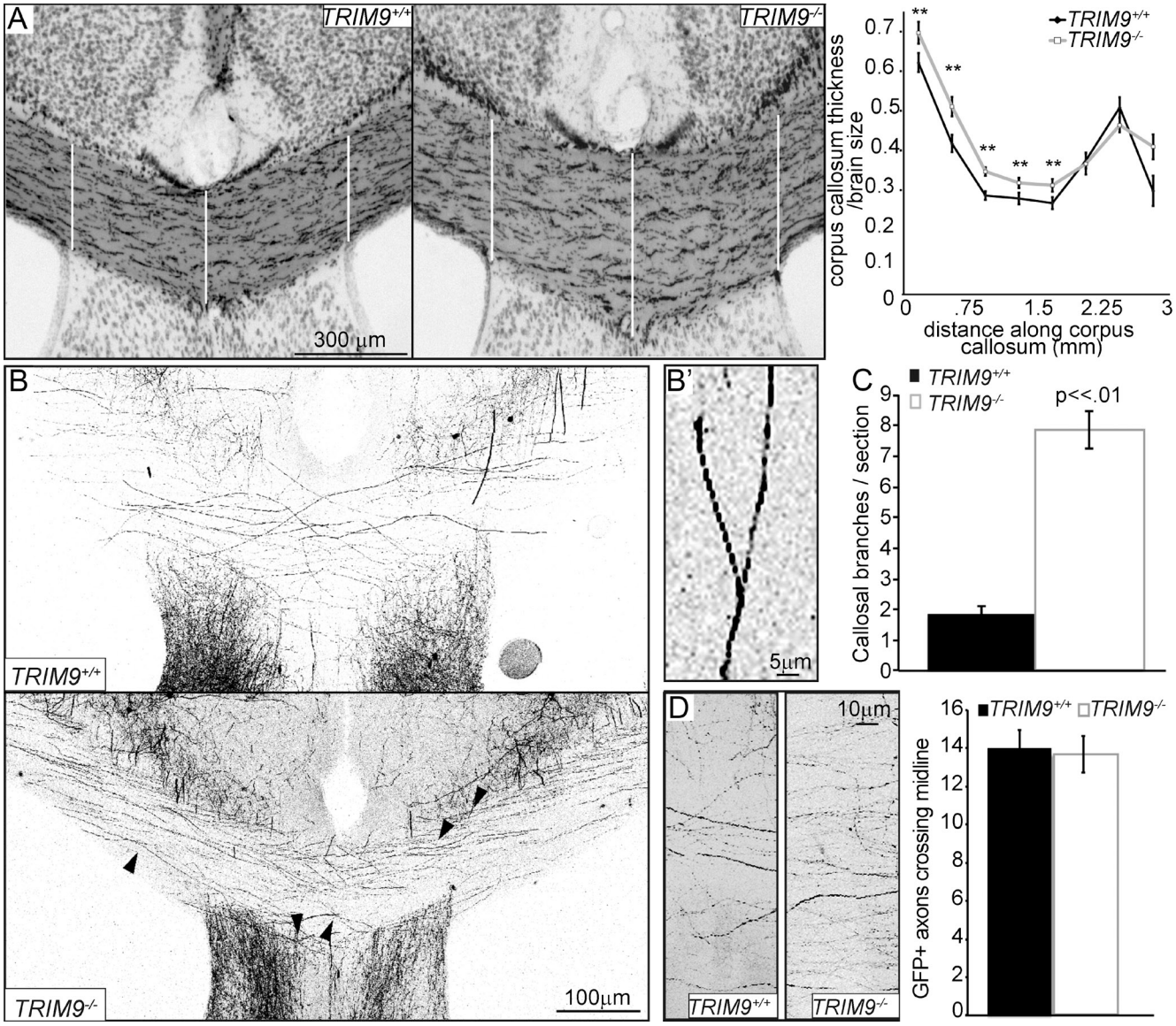

Figure 8. **Genetic loss of *TRIM9* leads to aberrant axon branching within and thickening of the corpus callosum.** (A) Coronal sections through corpus callosum from adult *TRIM9*$^{+/+}$ and *TRIM9*$^{-/-}$ mice stained for nissl substance. Lines denote callosal thickness measurements. Graph shows quantitation of callosal thickness; $n = 5$ mice/genotype; **, $P < 0.05$ obtained from *t* test. (B) Inverted maximal projections of Thy1-GFP/*TRIM9*$^{+/+}$ and *TRIM9*$^{-/-}$ corpus callosum sections. Arrowheads denote branch points. (B′) Inset shows an example of a branch. Video 6. (C) Quantitation of axonal branch points in 3-wk-old littermates; $n = 3$ mice/genotype. P-values obtained from *t* test. (D) Example images used in quantitation of the number of GFP-expressing axons crossing the midline in Thy1-GFP/*TRIM9*$^{+/+}$ and Thy1-GFP/*TRIM9*$^{-/-}$ brains. Error bars show SEMs.

allowing direct comparison of neuronal morphology. We selected a line in which <10% of cortical neurons express GFP (Feng et al., 2000) and compared callosal axon branching in *TRIM9*$^{+/+}$ and *TRIM9*$^{-/-}$ littermates (Fig. 8 B and Video 6). To confirm that littermates had comparable GFP expression and a similar number of GFP-expressing axons within the callosum, we quantified GFP-expressing axons in a 150 × 50–µm region at the midline. Although there was no difference in the number of GFP-expressing axons (Fig. 8 D) and no difference in the density of myelin within the corpus callosum (Fig. S5 C), Thy1-GFP/*TRIM9*$^{-/-}$ mice exhibited a fourfold increase in the number of axon branches within the callosum (Fig. 8 C and Video 6). This indicates that the exuberant branching observed in vitro also occurs in vivo and may underlie the thickened corpus callosum of *TRIM9*$^{-/-}$ mice.

Discussion

Our data delineate a molecular mechanism by which TRIM9 directly links Netrin-1/DCC signaling to the control of vesicle trafficking machinery required for local exocytosis, plasma membrane expansion, and axon branching (Fig. 9). We show that Netrin-1–dependent branching is preceded by an increase in SNARE complex formation and SNARE-mediated exocytosis and that this increase in exocytosis is both regulated by TRIM9 ligase activity and required for axon branch formation. TRIM9 binds to and colocalizes with DCC in cortical neurons, and TRIM9 catalytic activity is required to impart Netrin-1 sensitivity. The TRIM9 interaction with SNAP25 negatively regulates SNARE complex formation and SNARE-mediated exocytosis, but the interaction

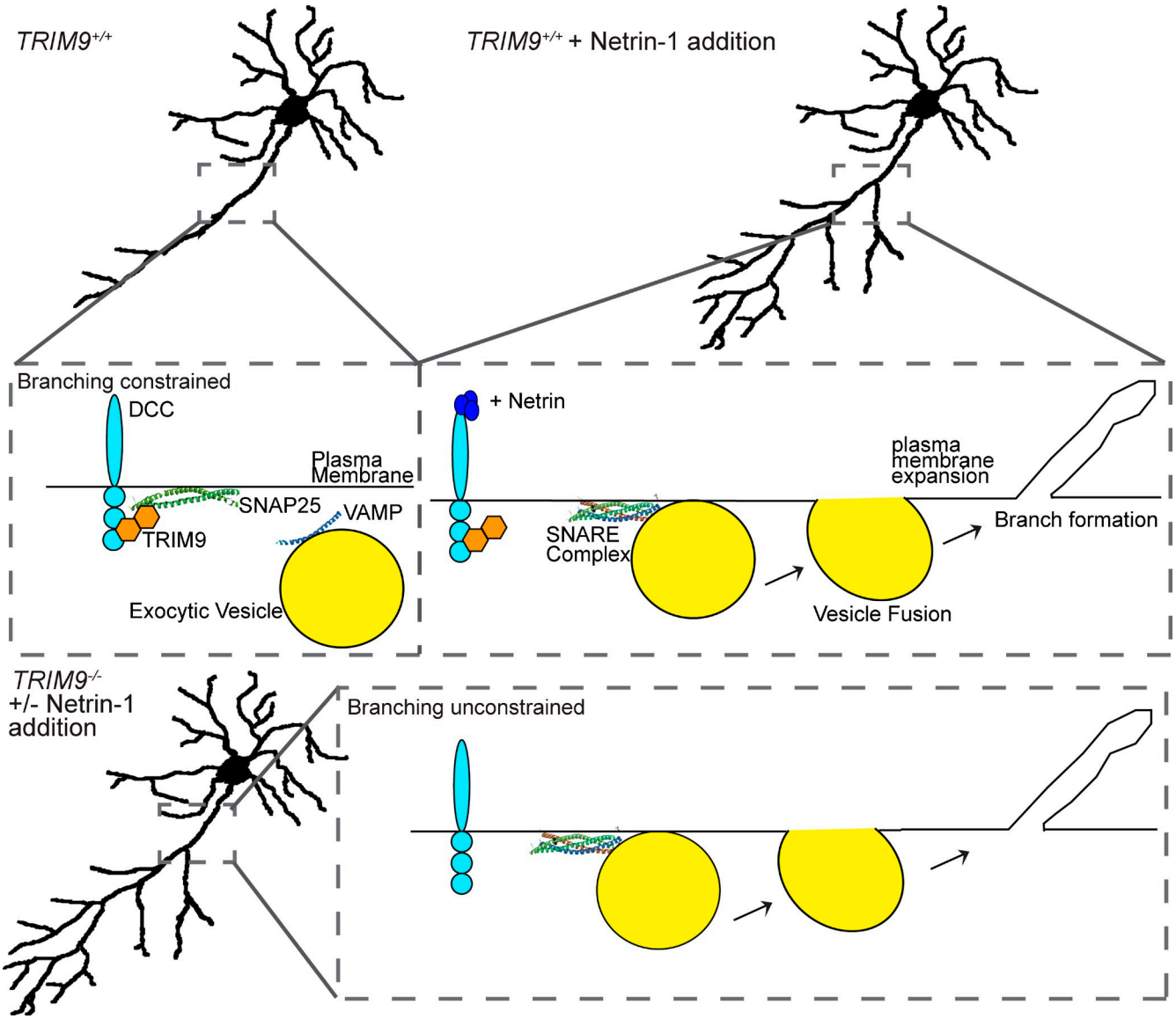

Figure 9. **Molecular mechanism of Netrin-1–dependent axon branching.** (top left) In the absence of Netrin-1, TRIM9 (orange) is bound to SNAP25 (green). The TRIM9 interaction blocks SNAP25 binding to VAMP2 or VAMP7 (blue), which inhibits SNARE complex formation and exocytic vesicle fusion. Prevention of plasma membrane expansion constrains basal levels of axon branching. (top right) After Netrin-1 stimulation, TRIM9 releases SNAP25, which promotes SNARE complex formation, vesicle fusion, local plasma membrane expansion, and axon branching. (bottom) Genetic deletion of *TRIM9* renders cells nonresponsive to Netrin-1. As the interaction between SNAP25 and VAMP2 or VAMP7 is no longer inhibited, constitutive levels of SNARE complex formation, exocytosis, and axon branching increase. To reduce and rescue the exocytosis and axon branching phenotypes associated with loss of *TRIM9*, introduction of TRIM9 containing the SNAP25 binding domain is required. To rescue Netrin-1 sensitivity, TRIM9 containing ubiquitin ligase activity must be introduced.

is disrupted in the presence of Netrin-1. This disruption promotes Netrin-1–dependent SNARE complex formation and exocytosis (Fig. 9). Our results identify TRIM9 as a Netrin-1–sensitive negative regulator of axon branching in vitro and in vivo, at least in part through control of SNAP25-mediated exocytosis. Surprisingly, the exaggerated branching displayed by *TRIM9*$^{-/-}$ neurons was strikingly dissimilar to the loss of branching in *madd-2/asap* mutants in invertebrates (Hao et al., 2010; Morikawa et al., 2011). Additionally, deletion of *TRIM9* does not phenocopy loss of *NTN1* or *DCC* in vivo as with invertebrate orthologues. This contrast in phenotypes between TRIM9 and its invertebrate orthologues suggests functional divergence of vertebrate TRIM9.

Multiple vesicle types provide membrane material required for axon branching

Netrin-1 stimulation in cortical neurons increases exocytosis mediated by VAMP2 and VAMP7. Both v-SNAREs form a SNARE complex with SNAP25 (Söllner et al., 1993; Martinez-Arca et al., 2000), which is consistent with our conclusion that TRIM9 regulates SNARE-mediated exocytosis through a Netrin-1–sensitive interaction with SNAP25. Because VAMP2 and VAMP7 mark distinct vesicle populations (Proux-Gillardeaux et al., 2005; Gupton and Gertler, 2010), these data indicate that TRIM9 promotes the insertion of multiple vesicular membrane sources into the plasma membrane in a Netrin-1–dependent manner. That these vesicles might deliver distinct cargoes or fuse in spatially segregated

regions of the axon is an intriguing possibility. Indeed, VAMP2 and VAMP7 have distinct exocytic behaviors during neuritogenesis and axon guidance (Tojima et al., 2007; Gupton and Gertler, 2010; Cotrufo et al., 2011). Whether dissimilarities stem from developmental stage, organismal, or neuronal subtype differences is unknown. However, DCC is associated with both VAMP2- and VAMP7-containing vesicles (Bouchard et al., 2004, 2008; Cotrufo et al., 2012); thus, Netrin-1–stimulated exocytosis may produce a positive feedback loop by delivering DCC to the plasma membrane.

Distinct roles for TRIM9 ubiquitin ligase activity and SNAP25 binding

TRIM proteins primarily mediate cellular functions through the ubiquitination of specific substrates. Although TRIM9 can autoubiquitinate (Tanji et al., 2010), its substrates in vivo remain unidentified. The results of our experiments using TRIM9ΔRING expression suggest that TRIM9 ligase activity is required for cortical neurons to release SNAP25 in response to Netrin-1 and promote exocytosis and axon branching. In contrast, the ligase domain was dispensable for binding to SNAP25 and constraining both exocytosis and axon branching in the absence of Netrin-1. Expression of TRIM9ΔRING did not induce a phenotype in *TRIM9*$^{+/+}$ neurons in the absence of Netrin-1. This is likely caused by the preexisting constraint of exocytosis and axon branching by endogenous TRIM9. Although the RING domain may provide only a structural role, the inhibition of Netrin-1–dependent axon branching observed in TRIM9LD-expressing neurons suggests that this is unlikely. Although ΔRING mutants are described as dominant negatives, TRIM9ΔRING partially maintained functions of TRIM9 and its expression did not fully phenocopy deletion of *TRIM9*. In contrast, in *C. elegans*, the expression of madd-2ΔRING phenocopied loss-of-function mutants (Hao et al., 2010). This further supports the possibility of the divergence of vertebrate TRIM9.

The CC domain of TRIM9 was required to minimize basal exocytosis and axon branching. We found that TRIM9ΔCC was impaired in SNAP25 binding and failed to reduce exocytosis and axon branching when expressed in *TRIM9*$^{-/-}$ neurons. Additionally, neurons expressing TRIM9ΔCC failed to respond to Netrin-1. Based on the failure of *TRIM9*$^{-/-}$ neurons to branch in response to FGF unless elevated axon branching was first reduced, we conclude that axon branching in *TRIM9*$^{-/-}$ neurons was maximized. Given this, the failure of the TRIM9ΔCC neurons to respond to Netrin-1 may result from a maximum level of branching and exocytosis in *TRIM9*$^{-/-}$ neurons. Surprisingly, expression of TRIM9ΔCC in *TRIM9*$^{+/+}$ neurons phenocopied the deletion of *TRIM9*. This suggests that TRIM9ΔCC inhibits the function of endogenous TRIM9 and acts as a dominant negative. Binding assays suggested that this likely did not occur through interaction with endogenous TRIM9; we suggest the dominant-negative effect occurs through TRIM9ΔCC sequestration of another TRIM9 binding partner required for the function of endogenous TRIM9, such as DCC. Alternatively, the ligase activity of TRIM9ΔCC may directly act on the substrate of TRIM9 to promote exocytosis and branching.

Integration of TRIM9 into established Netrin-1 signaling pathways

As DCC lacks catalytic motifs, its interaction partners are critical for the activation of signaling events and downstream cellular changes. Our findings indicate that TRIM9 represents a novel catalytic partner of DCC that directly affects Netrin-1–dependent neuronal behavior. Because TRIM proteins homodimerize (Short and Cox, 2006), TRIM9 dimers may promote the clustering and avidity of DCC within the plasma membrane, modulating DCC signaling in an inside-out fashion. By binding the cytoplasmic tail of DCC, TRIM9 may also modulate the binding of other partners of DCC, altering signaling in an outside-in fashion. The nonconventional myosin motor Myo10 also binds the cytoplasmic tail of DCC and targets DCC to the tips of neurites (Zhu et al., 2007; Wei et al., 2011). The dynamic colocalization of TRIM9 with DCC at the tips of neurites and filopodia suggests that TRIM9 may enhance Myo10 binding and transport of DCC.

TRIM9 function in other Netrin-1/DCC-dependent activities

Netrin-1 and DCC orchestrate filopodia dynamics during neural development (Lebrand et al., 2004). The prominent localization of TRIM9 at F-actin–rich filopodia tips suggests that TRIM9 may alter filopodial formation, function, or response to Netrin-1. Consistent with this, the invertebrate orthologues of *TRIM9* directly interact with and are required for localization of the evolutionarily conserved actin regulator *mig10* in response to netrin (Quinn et al., 2008; Hao et al., 2010; Michael et al., 2010; Morikawa et al., 2011). Whether TRIM9 regulates filopodia formation downstream of Netrin-1 through a conserved interaction with the vertebrate *mig10* orthologue Lamellipodin remains to be shown. Netrin-1 and DCC are also critical for the proper migration of neurons and commissure formation (Moore et al., 2007; Shi et al., 2008; Hakanen et al., 2011). Netrin-1 can be either a chemoattractant or chemorepulsive cue, dependent on whether DCC is in a complex with the repulsive receptor Unc5 (Hong et al., 1999). Therefore, loss of *TRIM9* may disrupt axon guidance and induce defects in axonal projections. Although we found that the thickening of the corpus callosum of *TRIM9*$^{-/-}$ mice correlated with increased axon branching, defective axon guidance may also underlie this phenotype. Indeed, disorganization of axons and an increased width of the portion of the callosum containing neuropilin-1–positive axons were observed in mice lacking *VAMP2*, which was proposed to result from aberrant axon repulsion to semaphorin-3 (Zylbersztejn et al., 2012). Netrin-1 and DCC also promote synaptogenesis and regulate plasticity (Goldman et al., 2013; Horn et al., 2013). Interestingly, a proteomic study identified TRIM9 at the synapse (Jordan et al., 2004). The ability of TRIM9 to control SNAP25-dependent exocytosis and its interaction with DCC make TRIM9 an attractive candidate to regulate synaptogenesis and synaptic function.

TRIM genes in neural development and function

The cerebral cortex controls cognitive function, sensory perception, and consciousness (Molyneaux et al., 2007), and thickening of the corpus callosum is associated with mental retardation

and other neuroanatomical anomalies (Göçmen and Oğuz, 2008; Lerman-Sagie et al., 2009). Although *TRIM9*$^{-/-}$ mice are viable, additional anatomical defects may occur, and the aberrant axon branching present in *TRIM9*$^{-/-}$ mice may disrupt synaptic targeting, resulting in behavioral changes. While there is a single class I TRIM gene in invertebrates, vertebrates contain six class I TRIM paralogues (Short and Cox, 2006). Whether one of these is functionally more similar to the invertebrate orthologues *madd-2/asap* than TRIM9 has not been investigated. Because some closely related TRIM proteins heterodimerize, the consequences of loss of *TRIM9* may extend beyond its own substrates and activities. Mutations in the class I family member *TRIM18* cause Opitz syndrome, in which patients are characterized by midline defects, neuroanatomical anomalies, and mental retardation (Quaderi et al., 1997; Gaudenz et al., 1998). The closest *TRIM18* paralogue, TRIM1, heterodimerizes with TRIM18 and modifies this disease (Short and Cox, 2006; Suzuki et al., 2010). *TRIM67* is the closest paralogue of *TRIM9* (Short and Cox, 2006), sharing 76% sequence similarity, and TRIM67 has been implicated in the extension of neuritelike processes (Yaguchi et al., 2012). Whether TRIM9 and TRIM67 heterodimerize or share overlapping expression patterns or substrates is unknown. If so, loss of both genes may produce more severe developmental or functional phenotypes than loss of *TRIM9* or *TRIM67* individually.

Materials and methods

Animals

All mouse lines were on a 129S4–C57BL/6 background and were bred at the Massachusetts Institute of Technology or University of North Carolina with approval from the Institutional Animal Care and Use Committee. Timed pregnant females were obtained by placing male and female mice together overnight; the following day was designated as E0.5 if the female had a vaginal plug.

Generation of *TRIM9*$^{-/-}$ mice

A conditional allele of *TRIM9* (*TRIM9*^{F}) was constructed by flanking exon 1, which encodes the RING and BBox domains of TRIM9, with LoxP sites. After Cre-mediated recombination, the subsequent 11 ATGs encode out-of-frame transcripts. The conditional TRIM9 targeting vector also contained a thymidine kinase–negative selection cassette and a Flippase recognition target–flanked phosphoglycerate kinase I–neomycin cassette. The *TRIM9*^{F} allele did not disrupt TRIM9 expression (not depicted), but exposure to Cre recombinase deleted exon 1 and abolished TRIM9 expression (Fig. S2). Embryonic stem cells were electroporated, selected, and screened for correct recombination and single integration. Two karyotyped, correctly targeted embryonic stem cell clones gave germline transmission and identical results. CMV-Cre mice (Jackson ImmunoResearch Laboratories, Inc.) were used to produce *TRIM9*$^{-/-}$ mice. Cre-mediated excision of exon 1 was confirmed by PCR genotyping.

Plasmids, antibodies, and reagents

Human TRIM9 cDNA (T. Cox, University of Washington, Seattle, WA), TRIM9ΔRING (aa 139–781), and TRIM9ΔCC (removed aa 220–394) were subcloned into pCs2+, pEGFP-C1, and mCherry-C1 (Takara Bio Inc.), under CMV promoters. TRIM9LD was cloned into pCS2+ using site-directed mutagenesis (QuikChange; Agilent Technologies) of Cys10 and Cys13 to alanine. TRIM9-SPRY (aa 576–693) was cloned into pGEX6P1 under a Taq promoter. pcDNA3.1-HA rat DCC under a CMV promoter was acquired from M. Tessier-Lavigne (The Rockefeller University, New York, NY). Rat DCC was cloned into mCherry-C1 under a CMV promoter with mCherry located within the extracellular domain of DCC between the Thr1041 and Leu1042. pEGFP-mouse VAMP2-pHluorin, pCax-human VAMP7-pHluorin, and pEGFP2-human VAMP7 N terminus (longin; aa 1–120) under CMV promoters were previously described (Gupton and Gertler, 2010). GST-SNAP25B (J. Rothman, Yale University, New Haven, CT) and pEGFP-SNAP25B under a CMV promoter (L. Chamberlain, University of Edinburgh, Edinburgh, Scotland, UK) were acquired. Antibodies include TRIM9 rabbit polyclonal (generated using murine TRIM9 recombinant protein aa 158–271), TRIM9 rabbit polyclonal (generated against the N terminus of human TRIM9; K. Wakabayashi, Hirosaki University, Hirosaki, Aomori, Japan; Tanji et al., 2010), mouse polyclonal against human TRIM9 (1F12; Abnova), mouse monoclonal c-Myc (9E10; Santa Cruz Biotechnology, Inc.), mouse monoclonal human DCC (G97-449; BD), rabbit polyclonal GST (G1417; Sigma-Aldrich), mouse monoclonal against human βIII-tubulin (Tuj-1; Santa Cruz Biotechnology, Inc.), rabbit polyclonal against GFP (A11122; Invitrogen), mouse monoclonal against HA (05–904; EMD Millipore), rabbit polyclonal against human VAMP2 (11829; Cell Signaling Technology), mouse monoclonal against rat Syntaxin-1a (HPC-1; Santa Cruz Biotechnology, Inc.), goat polyclonal against human SNAP25 (C-18; Santa Cruz Biotechnology, Inc.), and mouse monoclonal against GAPDH (sc-166545; Santa Cruz Biotechnology, Inc.). Fluorescent secondary antibodies and fluorescent phalloidin labeled with Alexa Fluor 488, Alexa Fluor 568, or Alexa Fluor 647 were obtained from Invitrogen. Recombinant Netrin-1 was concentrated from HEK293 cells (Serafini et al., 1994; Lebrand et al., 2004). Recombinant FGF2 (MBL International), TeNT (Sigma-Aldrich), and BoNTA (List Biological Laboratories, Inc.) were used as indicated.

Yeast two hybrid

LexA two-hybrid system selection with mouse Matchmaker cDNA library and β-galactosidase assays was performed according to the manufacturer's protocol (Takara Bio Inc.). DCC was used as bait in an embryonic mouse brain library.

Cortical neuron culture, transfection, and imaging

Cortical neuron cultures were prepared from day 15.5 embryos as previously described (Kwiatkowski et al., 2007). In brief, cortices were microdissected, and neurons were dissociated using trypsin and plated on poly-D-lysine (Sigma-Aldrich)–coated coverglass or tissue culture plastic in neurobasal media supplemented with b27 (Invitrogen). This same media were used for all time-lapse imaging experiments. For transfection, neurons were resuspended after dissociation in solution (Amaxa Nucleofector; Lonza) and electroporated with a Nucleofector according to manufacturer's protocol. For axon branching assays, 250 ng/ml Netrin-1 or 10 ng/ml FGF2 were bath applied after 48 h in culture. After 24 h of treatment, neurons were fixed in 4% paraformaldehyde, permeabilized for 10 min in 0.1% Triton X-100, blocked for 30 min in 10% BSA, and stained with indicated primary antibodies for 1 h at room temperatures as previously described (Strasser et al., 2004). After three washes, species-appropriate fluorescent secondary antibodies were incubated on coverslips for 1 h at room temperature. After three washes, cells were mounted in a Tris/glycerol/*n*-propyl-gallate–based mounting media for imaging. Images of pyramidal-shaped neurons were collected at room temperature on an inverted microscope (DeltaVision; Applied Precision) with a 20× U Apochromat/340, 0.75 NA or 60×, 1.3 NA Plan Apochromat objective lens (Olympus) and a charge-coupled device (CoolSNAP HQ; Photometrics) and deconvolved using softWoRx software (Applied Precision) or on an inverted microscope (IX81-ZDC2; Olympus) with a 40×, 1.4 NA Plan Apochromat objective lens (Olympus) and an electron multiplying charge-coupled device (iXon; Andor Technology) using MetaMorph acquisition software (Molecular Devices). Axon branches were defined as extensions off the primary axon that were ≥20 µm in length. Pearson's correlation of colocalization between TRIM9 and DCC was performed using regions of interest (ROIs) and an Intensity Correlation Analysis plugin for ImageJ (National Institutes of Health). All time-lapse imaging was performed on an inverted microscope (IX81-ZDC2) with MetaMorph acquisition software, an electron-multiplying charge-coupled device (iXon), and an imaging chamber (Stage Top Incubator INUG2-FSX; Tokai Hit), which maintained 37°C and 5% CO_2. For DIC time-lapse imaging, neurons were stimulated with 250 ng/ml Netrin-1 at 48 h, and images were acquired every 20 s with a 60× Plan Apochromat, 1.4 NA objective lens for 24 h. Images were analyzed in MetaMorph for the time after Netrin-1 stimulation of initial plasma membrane protrusion at sites that subsequently formed stable axon branches (20 µm long). For pHluorin assays, neurons expressing VAMP2-pHluorin or VAMP7-pHluorin and mCherryTRIM9 variants were imaged after 48 h in culture with a 100×, 1.49 NA TIRF objective and a solid-state 491-nm laser illumination at 100-nm penetration depth. Images were acquired every 0.5 s for 5 min. The frequency of exocytic events normalized per cell area and time is reported for the entire cell area in the image, soma, and neurite. 500 ng/ml Netrin-1 was added 1 h before imaging of Netirn-1–stimulated neurons. To emphasize pHluorin-based exocytic events, the mean

fluorescence intensity of the time lapse was subtracted from each frame, and images were inverted.

Immunoblotting and immunohistochemistry

SDS-PAGE and immunoblot analysis were performed using standard procedures with HRP secondary antibodies for GST-SPRY and endogenous TRIM9 (Jackson ImmunoResearch Laboratories, Inc.) or far-red–conjugated secondary antibodies (LI-COR Biosciences) for all other primary antibodies. Signal was detected using the ECL Plus (GE Healthcare) or an Odyssey Imager (LI-COR Biosciences), respectively. For neuroanatomical experiments, brains were placed in 4% paraformaldehyde, pH 7.2, in PBS for 24 h. Embryonic brains were mounted in 4% agarose, and 100-µm coronal sections were cut on a vibratome (VT1200; Leica) as previously described (Kwiatkowski et al., 2007). For immunohistochemistry, free-floating sections were permeabilized with 50% ethanol, treated for with 3% H_2O_2 in 0.1 M phosphate buffer, pH 7.4, and blocked in 10% normal donkey serum. Sections were incubated in primary antibody overnight and then for 3 h in biotinylated secondary antibody (Vector Laboratories) and for 1 h in ExtrAvidin-peroxidase (Sigma-Aldrich). Peroxidase was histochemically visualized with diaminobenzidine. Processed sections were mounted on gelatin-coated slides and imaged by transmitted light microscopy. For measuring callosal thickness, 50-µm-thick coronal sections of 3-mo-old mice were stained for nissl substance with 0.1% thionine, mounted using a Tris/glycerol/*n*-propyl-gallate–based mounting media, and imaged on a microscope (Leitz DMR; Leica; with cooled mono 12 bit charge-coupled device [Retiga EX; QImaging] with QImaging software) equipped with a Plan Fluotar 2.5×, 0.07 NA objective lens (Leica). In the second line of mice, 30-µm-thick coronal sections of 6-wk-old mice were stained with black gold II (Histo-Chem, Inc.) per manufacturer protocol and mounted in DPX mounting media (VWR International). Sections were imaged on a microscope (MVX10 MacroView; Olympus) equipped with MacroView Plan Apochromat 1×, 0.25 NA objective lens and a charge-coupled device (Orca-03G; Hamamatsu Photonics) using MetaMorph acquisition software. The mean intensity of black gold II staining per section in a 50 × 200–µm ROI at the midline was compared between genotypes.

Coimmunoprecipitation and binding assays

All coimmunoprecipitation assays were performed using standard procedures as previously described (Gupton et al., 2012). In brief, IgG-conjugated A/G beads (Santa Cruz Biotechnology, Inc.) were used to preclear lysates for 1.5 h at 4°C with agitation. Myc-conjugated A/G beads (Santa Cruz Biotechnology, Inc.) were agitated within precleared lysates for 2 h at 4°C to precipitate target proteins. For binding assays, all recombinant GST-tagged proteins were expressed in *Escherichia coli* strain BL21 (DE3) Codon Plus (Agilent Technologies) and purified by chromatography on Sepharose-immobilized glutathione beads (Thermo Fisher Scientific). For endogenous DCC binding, cortices were lysed in radioimmunoprecipitation assay buffer, precleared with GST-glutathione–Sepharose beads for 1 h at 4°C with agitation, and incubated with 5–10 µg of GST fusion protein or GST immobilized onto glutathione–Sepharose beads at 4°C overnight. For binding of Myc-tagged TRIM9 variants, HEK293 cells were transfected using Lipofectamine 2000 (Invitrogen) per manufacturer protocol, lysed in PBS buffer (140 mM NaCl, 2.7 mM KCl, 10 mM Na_2HPO_4, and 1.8 mM KH_2PO_4, pH 7.4 plus protease inhibitors, as described in Li et al., 2001), and agitated overnight at 4°C with 5 nM GST or GST-SNAP25. For both immunoprecipitation assays and GST-binding assays, beads were washed three times with lysis buffer, and bound proteins were resolved by SDS-PAGE and immunoblotting.

Peptide array

Peptides corresponding to 25-aa stretches in the murine DCC cytoplasmic tail (aa 1,012–1,447), overlapping by 3 aa in each progressive spot were covalently linked to a nitrocellulose membrane (Koch Institute Biopolymers Facility). The membrane was overlaid with recombinant GST-SPRY or GST alone, and protein binding was visualized using a GST antibody, secondary HRP antibody, and ECL.

SNARE complexes

SDS-resistant SNARE complexes were analyzed as previous described (Hayashi et al., 1994). In brief, E15.5 cortical neurons cultured 48 h were stimulated with 250 ng/ml Netrin-1 for 1 h before lysis, SDS-PAGE, and immunoblotting for SNARE proteins. SDS-resistant SNARE complexes were defined as immunoreactive material >40 kD present in samples incubated at 37°C compared with 100°C as previously described (Burré et al., 2010).

Laser-scanning confocal microscopy of Thy1-GFP corpus callosum

200-µm coronal sections of 30-wk-old Thy1-GFP, *TRIM9*$^{+/+}$, *and TRIM9*$^{-/-}$ littermates mounted in DPX mountant were imaged on a confocal inverted microscope (FluoView FV1200; Olympus) equipped with a 20×, 0.75 NA Plan Apochromat objective lens with a 488-nm argon laser. Multiarea z stacks were stitched, and ROIs containing potential axon branch points were identified in maximal projections. Candidate branches were confirmed by inspection of stitched z stacks. The mean number of branches ± SEM within the corpus callosum per section is reported. The mean number ± SEM of GFP$^+$ axons crossing the callosum in a 150 × 50–µm ROI from the maximum projection images was reported.

Statistics

At least three independent experiments were performed for each assay. Statistical tests used are indicated in the legends. Two independent, normally distributed samples were compared using unpaired *t* tests. For greater than two conditions, Kruskal–Wallis nonparametric analysis of variance (ANOVA) was performed in samples lacking normal distribution, as ascertained by a Fisher test. In normally distributed samples, ANOVA with Tukey's post-hoc correction were used. P-values are listed in figures or figure legends, which present means with SEM.

Online supplemental material

Fig. S1 shows TRIM9 localization and interaction. Fig. S2 details the generation of *TRIM9*$^{-/-}$ mice and confirms gene deletion and loss of protein. Fig. S3 contains representative images from Netrin-1 branching assays that show that TRIM9 ligase activity is necessary to rescue axon branching defects in *TRIM9*$^{-/-}$ neurons. Fig. S4 provides details of SNARE complex formation and confirms that TRIM9 ligase activity is required to promote Netrin-1–dependent exocytosis and release of SNAP25. Fig. S5 reaffirms that genetic loss of *TRIM9* results in thickening of the corpus callosum in an independently targeted line of *TRIM9*$^{-/-}$ mice. Video 1 reveals the dynamic colocalization of GFP-TRIM9 and mCherry-DCC. Video 2 shows Netrin-1–induced increases in VAMP2-mediated exocytosis in a *TRIM9*$^{+/+}$ cortical neuron. Video 3 shows increases in VAMP2-mediated exocytosis in a *TRIM9*$^{-/-}$ cortical neuron independent of Netrin-1 stimulation. Video 4 illustrates the time course of plasma membrane protrusion and axon branching in a *TRIM9*$^{+/+}$ cortical neuron after Netrin-1 stimulation. Video 5 shows that expression of TRIM9ΔCC does not rescue the elevated VAMP2-mediated exocytosis of *TRIM9*$^{-/-}$ cortical neurons. Video 6 shows aberrant axon branching within the Thy1-GFP/*TRIM9*$^{-/-}$ corpus callosum. Online supplemental material is available at http://www.jcb.org/cgi/content/full/jcb.201311003/DC1. Additional data are available in the JCB DataViewer at http://dx.doi.org/10.1083/jcb.201311003.dv.

We thank Richard Weinberg, Patrick Brennwald, and the Gupton laboratory for thoughtful critique of the manuscript. We thank Doug Rubinson for helpful guidance. We thank the Rippel and Biopolymers facilities at the Massachusetts Institute of Technology and the Olympus Center and Robert Currin at the University of North Carolina as well as Jenny Tadros, Christopher Bott, and Hieu Nguyen for technical assistance.

This work was supported by National Institutes of Health grant GM108970 (S.L. Gupton), the Lineberger Comprehensive Cancer Center at the University of North Carolina at Chapel Hill School of Medicine (S.L. Gupton), and an American Heart Association fellowship 0615692T (L.M. McClain). The work performed at the Massachusetts Institute of Technology was supported by National Institutes of Health grant GM68678 to Frank Gertler, whom we thank for generous support and invaluable discussions.

The authors declare no competing financial interests.

Submitted: 1 November 2013
Accepted: 24 March 2014

References

Alexander, M., G. Selman, A. Seetharaman, K.K.M. Chan, S.A. D'Souza, A.B. Byrne, and P.J. Roy. 2010. MADD-2, a homolog of the Opitz syndrome protein MID1, regulates guidance to the midline through UNC-40 in *Caenorhabditis elegans*. *Dev. Cell*. 18:961–972. http://dx.doi.org/10.1016/j.devcel.2010.05.016

Arlotta, P., B.J. Molyneaux, J. Chen, J. Inoue, R. Kominami, and J.D. Macklis. 2005. Neuronal subtype-specific genes that control corticospinal motor neuron development in vivo. *Neuron*. 45:207–221. http://dx.doi.org/10.1016/j.neuron.2004.12.036

Balastik, M., F. Ferraguti, A. Pires-da Silva, T.H. Lee, G. Alvarez-Bolado, K.P. Lu, and P. Gruss. 2008. Deficiency in ubiquitin ligase TRIM2

causes accumulation of neurofilament light chain and neurodegeneration. *Proc. Natl. Acad. Sci. USA*. 105:12016–12021. http://dx.doi.org/10.1073/pnas.0802261105

Berti, C., S. Messali, A. Ballabio, A. Reymond, and G. Meroni. 2002. TRIM9 is specifically expressed in the embryonic and adult nervous system. *Mech. Dev.* 113:159–162. http://dx.doi.org/10.1016/S0925-4773(02)00013-8

Bouchard, J.-F., S.W. Moore, N.X. Tritsch, P.P. Roux, M. Shekarabi, P.A. Barker, and T.E. Kennedy. 2004. Protein kinase A activation promotes plasma membrane insertion of DCC from an intracellular pool: A novel mechanism regulating commissural axon extension. *J. Neurosci.* 24:3040–3050. http://dx.doi.org/10.1523/JNEUROSCI.4934-03.2004

Bouchard, J.-F., K.E. Horn, T. Stroh, and T.E. Kennedy. 2008. Depolarization recruits DCC to the plasma membrane of embryonic cortical neurons and enhances axon extension in response to netrin-1. *J. Neurochem.* 107:398–417. http://dx.doi.org/10.1111/j.1471-4159.2008.05609.x

Burré, J., M. Sharma, T. Tsetsenis, V. Buchman, M.R. Etherton, and T.C. Südhof. 2010. Alpha-synuclein promotes SNARE-complex assembly in vivo and in vitro. *Science*. 329:1663–1667. http://dx.doi.org/10.1126/science.1195227

Cotrufo, T., F. Pérez-Brangulí, A. Muhaisen, O. Ros, R. Andrés, T. Baeriswyl, G. Fuschini, T. Tarrago, M. Pascual, J. Ureña, et al. 2011. A signaling mechanism coupling netrin-1/deleted in colorectal cancer chemoattraction to SNARE-mediated exocytosis in axonal growth cones. *J. Neurosci.* 31:14463–14480. http://dx.doi.org/10.1523/JNEUROSCI.3018-11.2011

Cotrufo, T., R.M. Andrés, O. Ros, F. Pérez-Brangulí, A. Muhaisen, G. Fuschini, R. Martínez, M. Pascual, J.X. Comella, and E. Soriano. 2012. Syntaxin 1 is required for DCC/Netrin-1-dependent chemoattraction of migrating neurons from the lower rhombic lip. *Eur. J. Neurosci.* 36:3152–3164. http://dx.doi.org/10.1111/j.1460-9568.2012.08259.x

Dent, E.W., A.M. Barnes, F. Tang, and K. Kalil. 2004. Netrin-1 and semaphorin 3A promote or inhibit cortical axon branching, respectively, by reorganization of the cytoskeleton. *J. Neurosci.* 24:3002–3012. http://dx.doi.org/10.1523/JNEUROSCI.4963-03.2004

Drachman, D.A. 2005. Do we have brain to spare? *Neurology*. 64:2004–2005. http://dx.doi.org/10.1212/01.WNL.0000166914.38327.BB

Fazeli, A., S.L. Dickinson, M.L. Hermiston, R.V. Tighe, R.G. Steen, C.G. Small, E.T. Stoeckli, K. Keino-Masu, M. Masu, H. Rayburn, et al. 1997. Phenotype of mice lacking functional Deleted in colorectal cancer (Dcc) gene. *Nature*. 386:796–804. http://dx.doi.org/10.1038/386796a0

Feng, G., R.H. Mellor, M. Bernstein, C. Keller-Peck, Q.T. Nguyen, M. Wallace, J.M. Nerbonne, J.W. Lichtman, and J.R. Sanes. 2000. Imaging neuronal subsets in transgenic mice expressing multiple spectral variants of GFP. *Neuron*. 28:41–51. http://dx.doi.org/10.1016/S0896-6273(00)00084-2

Gaudenz, K., E. Roessler, N. Quaderi, B. Franco, G. Feldman, D.L. Gasser, B. Wittwer, J. Horst, E. Montini, J.M. Opitz, et al. 1998. Opitz G/BBB syndrome in Xp22: mutations in the MID1 gene cluster in the carboxy-terminal domain. *Am. J. Hum. Genet.* 63:703–710. http://dx.doi.org/10.1086/302010

Göçmen, R., and K.K. Oğuz. 2008. Mega corpus callosum and caudate nuclei with bilateral hippocampal malformation. *Diagn. Interv. Radiol.* 14:69–71.

Goldman, J.S., M.A. Ashour, M.H. Magdesian, N.X. Tritsch, S.N. Harris, N. Christofi, R. Chemali, Y.E. Stern, G. Thompson-Steckel, P. Gris, et al. 2013. Netrin-1 promotes excitatory synaptogenesis between cortical neurons by initiating synapse assembly. *J. Neurosci.* 33:17278–17289. http://dx.doi.org/10.1523/JNEUROSCI.1085-13.2013

Grant, A., F. Fathalli, G. Rouleau, R. Joober, and C. Flores. 2012. Association between schizophrenia and genetic variation in DCC: a case-control study. *Schizophr. Res.* 137:26–31. http://dx.doi.org/10.1016/j.schres.2012.02.023

Gupton, S.L., and F.B. Gertler. 2010. Integrin signaling switches the cytoskeletal and exocytic machinery that drives neuritogenesis. *Dev. Cell*. 18:725–736. http://dx.doi.org/10.1016/j.devcel.2010.02.017

Gupton, S.L., D. Riquelme, S.K. Hughes-Alford, J. Tadros, S.S. Rudina, R.O. Hynes, D. Lauffenburger, and F.B. Gertler. 2012. Mena binds α5 integrin directly and modulates α5β1 function. *J. Cell Biol.* 198:657–676. http://dx.doi.org/10.1083/jcb.201202079

Hakanen, J., S. Duprat, and M. Salminen. 2011. Netrin1 is required for neural and glial precursor migrations into the olfactory bulb. *Dev. Biol.* 355:101–114. http://dx.doi.org/10.1016/j.ydbio.2011.04.016

Hämäläinen, R.H., K. Avela, J.A. Lambert, J. Kallijärvi, W. Eyaid, J. Gronau, A.P. Ignaszewski, D. McFadden, G. Sorge, M. Lipsanen-Nyman, and A.-E. Lehesjoki. 2004. Novel mutations in the TRIM37 gene in Mulibrey Nanism. *Hum. Mutat.* 23:522. http://dx.doi.org/10.1002/humu.9233

Hao, J.C., C.E. Adler, L. Mebane, F.B. Gertler, C.I. Bargmann, and M. Tessier-Lavigne. 2010. The tripartite motif protein MADD-2 functions with the receptor UNC-40 (DCC) in Netrin-mediated axon attraction and branching. *Dev. Cell*. 18:950–960. http://dx.doi.org/10.1016/j.devcel.2010.02.019

Hatakeyama, S. 2011. TRIM proteins and cancer. *Nat. Rev. Cancer*. 11:792–804. http://dx.doi.org/10.1038/nrc3139

Hayashi, T., H. McMahon, S. Yamasaki, T. Binz, Y. Hata, T.C. Südhof, and H. Niemann. 1994. Synaptic vesicle membrane fusion complex: action of clostridial neurotoxins on assembly. *EMBO J.* 13:5051–5061.

Hong, K., L. Hinck, M. Nishiyama, M.M. Poo, M. Tessier-Lavigne, and E. Stein. 1999. A ligand-gated association between cytoplasmic domains of UNC5 and DCC family receptors converts netrin-induced growth cone attraction to repulsion. *Cell*. 97:927–941. http://dx.doi.org/10.1016/S0092-8674(00)80804-1

Horn, K.E., S.D. Glasgow, D. Gobert, S.-J. Bull, T. Luk, J. Girgis, M.-E. Tremblay, D. McEachern, J.-F. Bouchard, M. Haber, et al. 2013. DCC expression by neurons regulates synaptic plasticity in the adult brain. *Cell Rep.* 3:173–185. http://dx.doi.org/10.1016/j.celrep.2012.12.005

Hung, A.Y., C.C. Sung, I.L. Brito, and M. Sheng. 2010. Degradation of postsynaptic scaffold GKAP and regulation of dendritic spine morphology by the TRIM3 ubiquitin ligase in rat hippocampal neurons. *PLoS ONE*. 5:e9842. http://dx.doi.org/10.1371/journal.pone.0009842

Joazeiro, C.A.P., and A.M. Weissman. 2000. RING finger proteins: mediators of ubiquitin ligase activity. *Cell*. 102:549–552. http://dx.doi.org/10.1016/S0092-8674(00)00077-5

Jordan, B.A., B.D. Fernholz, M. Boussac, C. Xu, G. Grigorean, E.B. Ziff, and T.A. Neubert. 2004. Identification and verification of novel rodent postsynaptic density proteins. *Mol. Cell. Proteomics*. 3:857–871. http://dx.doi.org/10.1074/mcp.M400045-MCP200

Kennedy, T.E., and M. Tessier-Lavigne. 1995. Guidance and induction of branch formation in developing axons by target-derived diffusible factors. *Curr. Opin. Neurobiol.* 5:83–90. http://dx.doi.org/10.1016/0959-4388(95)80091-3

Kubbutat, M.H., and K.H. Vousden. 1997. Proteolytic cleavage of human p53 by calpain: a potential regulator of protein stability. *Mol. Cell. Biol.* 17:460–468.

Kwiatkowski, A.V., D.A. Rubinson, E.W. Dent, J. Edward van Veen, J.D. Leslie, J. Zhang, L.M. Mebane, U. Philippar, E.M. Pinheiro, A.A. Burds, et al. 2007. Ena/VASP Is Required for neuritogenesis in the developing cortex. *Neuron*. 56:441–455. http://dx.doi.org/10.1016/j.neuron.2007.09.008

Lebrand, C., E.W. Dent, G.A. Strasser, L.M. Lanier, M. Krause, T.M. Svitkina, G.G. Borisy, and F.B. Gertler. 2004. Critical role of Ena/VASP proteins for filopodia formation in neurons and in function downstream of netrin-1. *Neuron*. 42:37–49. http://dx.doi.org/10.1016/S0896-6273(04)00108-4

Lerman-Sagie, T., L. Ben-Sira, R. Achiron, L. Schreiber, G. Hermann, D. Lev, D. Kidron, and G. Malinger. 2009. Thick fetal corpus callosum: an ominous sign? *Ultrasound Obstet. Gynecol.* 34:55–61. http://dx.doi.org/10.1002/uog.6356

Leyva-Díaz, E., and G. López-Bendito. 2013. In and out from the cortex: development of major forebrain connections. *Neuroscience*. 254:26–44. http://dx.doi.org/10.1016/j.neuroscience.2013.08.070

Li, Y., L.S. Chin, C. Weigel, and L. Li. 2001. Spring, a novel RING finger protein that regulates synaptic vesicle exocytosis. *J. Biol. Chem.* 276:40824–40833. http://dx.doi.org/10.1074/jbc.M106141200

Martinez-Arca, S., P. Alberts, A. Zahraoui, D. Louvard, and T. Galli. 2000. Role of tetanus neurotoxin insensitive vesicle-associated membrane protein (TI-VAMP) in vesicular transport mediating neurite outgrowth. *J. Cell Biol.* 149:889–900. http://dx.doi.org/10.1083/jcb.149.4.889

Meroni, G., and G. Diez-Roux. 2005. TRIM/RBCC, a novel class of 'single protein RING finger' E3 ubiquitin ligases. *Bioessays*. 27:1147–1157. http://dx.doi.org/10.1002/bies.20304

Michael, M., A. Vehlow, C. Navarro, and M. Krause. 2010. c-Abl, Lamellipodin, and Ena/VASP proteins cooperate in dorsal ruffling of fibroblasts and axonal morphogenesis. *Curr. Biol.* 20:783–791. http://dx.doi.org/10.1016/j.cub.2010.03.048

Miesenböck, G., D.A. De Angelis, and J.E. Rothman. 1998. Visualizing secretion and synaptic transmission with pH-sensitive green fluorescent proteins. *Nature*. 394:192–195. http://dx.doi.org/10.1038/28190

Molyneaux, B.J., P. Arlotta, J.R.L. Menezes, and J.D. Macklis. 2007. Neuronal subtype specification in the cerebral cortex. *Nat. Rev. Neurosci.* 8:427–437. http://dx.doi.org/10.1038/nrn2151

Moore, S.W., M. Tessier-Lavigne, and T.E. Kennedy. 2007. Netrins and their receptors. *Adv. Exp. Med. Biol.* 621:17–31. http://dx.doi.org/10.1007/978-0-387-76715-4_2

Morikawa, R.K., T. Kanamori, K.-I. Yasunaga, and K. Emoto. 2011. Different levels of the Tripartite motif protein, Anomalies in sensory axon patterning (Asap), regulate distinct axonal projections of *Drosophila* sensory neurons. *Proc. Natl. Acad. Sci. USA*. 108:19389–19394. http://dx.doi.org/10.1073/pnas.1109843108

Pfenninger, K.H. 2009. Plasma membrane expansion: a neuron's Herculean task. *Nat. Rev. Neurosci.* 10:251–261. http://dx.doi.org/10.1038/nrn2593

Proux-Gillardeaux, V., R. Rudge, and T. Galli. 2005. The tetanus neurotoxin-sensitive and insensitive routes to and from the plasma membrane: fast and slow pathways? *Traffic*. 6:366–373. http://dx.doi.org/10.1111/j.1600-0854.2005.00288.x

Quaderi, N.A., S. Schweiger, K. Gaudenz, B. Franco, E.I. Rugarli, W. Berger, G.J. Feldman, M. Volta, G. Andolfi, S. Gilgenkrantz, et al. 1997. Opitz G/BBB syndrome, a defect of midline development, is due to mutations in a new RING finger gene on Xp22. *Nat. Genet.* 17:285–291. http://dx.doi.org/10.1038/ng1197-285

Quinn, C.C., D.S. Pfeil, and W.G. Wadsworth. 2008. CED-10/Rac1 mediates axon guidance by regulating the asymmetric distribution of MIG-10/lamellipodin. *Curr. Biol.* 18:808–813. http://dx.doi.org/10.1016/j.cub.2008.04.050

Reuss, B., and O. von Bohlen und Halbach. 2003. Fibroblast growth factors and their receptors in the central nervous system. *Cell Tissue Res.* 313:139–157. http://dx.doi.org/10.1007/s00441-003-0756-7

Round, J., and E. Stein. 2007. Netrin signaling leading to directed growth cone steering. *Curr. Opin. Neurobiol.* 17:15–21. http://dx.doi.org/10.1016/j.conb.2007.01.003

Saccone, V., M. Palmieri, L. Passamano, G. Piluso, G. Meroni, L. Politano, and V. Nigro. 2008. Mutations that impair interaction properties of TRIM32 associated with limb-girdle muscular dystrophy 2H. *Hum. Mutat.* 29:240–247. http://dx.doi.org/10.1002/humu.20633

Schiavo, G., F. Benfenati, B. Poulain, O. Rossetto, P. Polverino de Laureto, B.R. DasGupta, and C. Montecucco. 1992. Tetanus and botulinum-B neurotoxins block neurotransmitter release by proteolytic cleavage of synaptobrevin. *Nature*. 359:832–835. http://dx.doi.org/10.1038/359832a0

Schiavo, G., O. Rossetto, S. Catsicas, P. Polverino de Laureto, B.R. DasGupta, F. Benfenati, and C. Montecucco. 1993. Identification of the nerve terminal targets of botulinum neurotoxin serotypes A, D, and E. *J. Biol. Chem.* 268:23784–23787.

Serafini, T., T.E. Kennedy, M.J. Galko, C. Mirzayan, T.M. Jessell, and M. Tessier-Lavigne. 1994. The netrins define a family of axon outgrowth-promoting proteins homologous to *C. elegans* UNC-6. *Cell*. 78:409–424. http://dx.doi.org/10.1016/0092-8674(94)90420-0

Serafini, T., S.A. Colamarino, E.D. Leonardo, H. Wang, R. Beddington, W.C. Skarnes, and M. Tessier-Lavigne. 1996. Netrin-1 is required for commissural axon guidance in the developing vertebrate nervous system. *Cell*. 87:1001–1014. http://dx.doi.org/10.1016/S0092-8674(00)81795-X

Shi, M., C. Guo, J.-X. Dai, and Y.-Q. Ding. 2008. DCC is required for the tangential migration of noradrenergic neurons in locus coeruleus of mouse brain. *Mol. Cell. Neurosci.* 39:529–538. http://dx.doi.org/10.1016/j.mcn.2008.07.023

Short, K.M., and T.C. Cox. 2006. Subclassification of the RBCC/TRIM superfamily reveals a novel motif necessary for microtubule binding. *J. Biol. Chem.* 281:8970–8980. http://dx.doi.org/10.1074/jbc.M512755200

Söllner, T., M.K. Bennett, S.W. Whiteheart, R.H. Scheller, and J.E. Rothman. 1993. A protein assembly-disassembly pathway in vitro that may correspond to sequential steps of synaptic vesicle docking, activation, and fusion. *Cell*. 75:409–418. http://dx.doi.org/10.1016/0092-8674(93)90376-2

Srour, M., J.-B. Rivière, J.M.T. Pham, M.-P. Dubé, S. Girard, S. Morin, P.A. Dion, G. Asselin, D. Rochefort, P. Hince, et al. 2010. Mutations in DCC cause congenital mirror movements. *Science*. 328:592. http://dx.doi.org/10.1126/science.1186463

Strasser, G.A., N.A. Rahim, K.E. VanderWaal, F.B. Gertler, and L.M. Lanier. 2004. Arp2/3 is a negative regulator of growth cone translocation. *Neuron*. 43:81–94. http://dx.doi.org/10.1016/j.neuron.2004.05.015

Südhof, T.C. 2012. The presynaptic active zone. *Neuron*. 75:11–25. http://dx.doi.org/10.1016/j.neuron.2012.06.012

Suzuki, M., Y. Hara, C. Takagi, T.S. Yamamoto, and N. Ueno. 2010. MID1 and MID2 are required for Xenopus neural tube closure through the regulation of microtubule organization. *Development*. 137:2329–2339. http://dx.doi.org/10.1242/dev.048769

Swann, J.W., and J.J. Hablitz. 2000. Cellular abnormalities and synaptic plasticity in seizure disorders of the immature nervous system. *Ment. Retard. Dev. Disabil. Res. Rev.* 6:258–267. http://dx.doi.org/10.1002/1098-2779(2000)6:4<258::AID-MRDD5>3.0.CO;2-H

Tanji, K., T. Kamitani, F. Mori, A. Kakita, H. Takahashi, and K. Wakabayashi. 2010. TRIM9, a novel brain-specific E3 ubiquitin ligase, is repressed in the brain of Parkinson's disease and dementia with Lewy bodies. *Neurobiol. Dis.* 38:210–218. http://dx.doi.org/10.1016/j.nbd.2010.01.007

Tojima, T., H. Akiyama, R. Itofusa, Y. Li, H. Katayama, A. Miyawaki, and H. Kamiguchi. 2007. Attractive axon guidance involves asymmetric membrane transport and exocytosis in the growth cone. *Nat. Neurosci.* 10:58–66. http://dx.doi.org/10.1038/nn1814

Tursun, B., A. Schlüter, M.A. Peters, B. Viehweger, H.P. Ostendorff, J. Soosairajah, A. Drung, M. Bossenz, S.A. Johnsen, M. Schweizer, et al. 2005. The ubiquitin ligase Rnf6 regulates local LIM kinase 1 levels in axonal growth cones. *Genes Dev.* 19:2307–2319. http://dx.doi.org/10.1101/gad.1340605

Wei, Z., J. Yan, Q. Lu, L. Pan, and M. Zhang. 2011. Cargo recognition mechanism of myosin X revealed by the structure of its tail MyTH4-FERM tandem in complex with the DCC P3 domain. *Proc. Natl. Acad. Sci. USA*. 108:3572–3577. http://dx.doi.org/10.1073/pnas.1016567108

Yaguchi, H., F. Okumura, H. Takahashi, T. Kano, H. Kameda, M. Uchigashima, S. Tanaka, M. Watanabe, H. Sasaki, and S. Hatakeyama. 2012. TRIM67 protein negatively regulates Ras activity through degradation of 80K-H and induces neuritogenesis. *J. Biol. Chem.* 287:12050–12059. http://dx.doi.org/10.1074/jbc.M111.307678

Yang, Y., S. Fang, J.P. Jensen, A.M. Weissman, and J.D. Ashwell. 2000. Ubiquitin protein ligase activity of IAPs and their degradation in proteasomes in response to apoptotic stimuli. *Science*. 288:874–877. http://dx.doi.org/10.1126/science.288.5467.874

Zechel, S., S. Werner, K. Unsicker, and O. von Bohlen und Halbach. 2010. Expression and functions of fibroblast growth factor 2 (FGF-2) in hippocampal formation. *Neuroscientist*. 16:357–373. http://dx.doi.org/10.1177/1073858410371513

Zhu, X.-J., C.-Z. Wang, P.-G. Dai, Y. Xie, N.-N. Song, Y. Liu, Q.-S. Du, L. Mei, Y.-Q. Ding, and W.-C. Xiong. 2007. Myosin X regulates netrin receptors and functions in axonal path-finding. *Nat. Cell Biol.* 9:184–192. http://dx.doi.org/10.1038/ncb1535

Zikopoulos, B., and H. Barbas. 2013. Altered neural connectivity in excitatory and inhibitory cortical circuits in autism. *Front Hum. Neurosci.* 7:609. http://dx.doi.org/10.3389/fnhum.2013.00609

Zylbersztejn, K., M. Petkovic, A. Burgo, M. Deck, S. Garel, S. Marcos, E. Bloch-Gallego, F. Nothias, G. Serini, D. Bagnard, et al. 2012. The vesicular SNARE Synaptobrevin is required for Semaphorin 3A axonal repulsion. *J. Cell Biol.* 196:37–46. http://dx.doi.org/10.1083/jcb.201106113